Molecular Therapy
Original Article

Sectm1a Facilitates Protection against Inflammation-Induced Organ Damage through Promoting TRM Self-Renewal

Xingjiang Mu,[1] Hongkuan Fan,[2] Peng Wang,[1] Yutian Li,[1] Karen Domenico,[3] Qianqian Li,[1] Xiaohong Wang,[1] Kobina Essandoh,[4] Jing Chen,[5] Tianqing Peng,[6] and Guo-Chang Fan[1]

[1]Pharmacology and Systems Physiology, University of Cincinnati College of Medicine, Cincinnati, OH 45267, USA; [2]Department of Pathology and Laboratory Medicine, Medical University of South Carolina, Charleston, SC 29425, USA; [3]Research Flow Cytometry Core, Cincinnati Children's Hospital Medical Center, Cincinnati, OH 45229-3026, USA; [4]Department of Pharmacology, University of Michigan Medical School, Ann Arbor, MI 48109-5632, USA; [5]UC Department of Pediatrics, UC Department of Biomedical Informatics, University of Cincinnati, Cincinnati, OH 45267-0575, USA; [6]Critical Illness Research, Lawson Health Research Institute, London, ON N6A 4G5, Canada

Tissue-resident macrophages (TRMs) are sentinel cells for maintaining tissue homeostasis and organ function. In this study, we discovered that lipopolysaccharide (LPS) administration dramatically reduced TRM populations and suppressed their self-renewal capacities in multiple organs. Using loss- and gain-of-function approaches, we define Sectm1a as a novel regulator of TRM self-renewal. Specifically, at the earlier stage of endotoxemia, Sectm1a deficiency exaggerated acute inflammation-induced reduction of TRM numbers in multiple organs by suppressing their proliferation, which was associated with more infiltrations of inflammatory monocytes/neutrophils and more serious organ damage. By contrast, administration of recombinant Sectm1a enhanced TRM populations and improved animal survival upon endotoxin challenge. Mechanistically, we identified that Sectm1a-induced upregulation in the self-renewal capacity of TRM is dependent on GITR-activated T helper cell expansion and cytokine production. Meanwhile, we found that TRMs may play an important role in protecting local vascular integrity during endotoxemia. Our study demonstrates that Sectm1a contributes to stabling TRM populations through maintaining their self-renewal capacities, which benefits the host immune response to acute inflammation. Therefore, Sectm1a may serve as a new therapeutic agent for the treatment of inflammatory diseases.

INTRODUCTION

Sepsis, as a systemic inflammatory disease, remains a major challenge for worldwide healthcare systems, with 31.5 million cases of sepsis and 19.4 million cases of severe sepsis occurring annually in high-income countries.[1,2] Notably, sepsis accounts for more than 50% of hospital deaths and has a considerable economic impact (13% of total US hospital costs).[3,4] Endotoxin (lipopolysaccharide [LPS]) is recognized as the most potent microbial mediator implicated in the pathogenesis of septic shock.[5,6]

As a fundamental component of innate immunity, macrophages are the most abundant immune cells in many tissues and the first responders to local damage or inflammation, and they play essential roles throughout all phases of inflammation disease.[7,8] The long-held belief that all macrophages are terminally differentiated immune cells derived from circulating monocyte infiltration has been challenged by recent evidence showing that most TRM (tissue-resident macrophage) populations originate from embryonic progenitors, persist into adulthood, and self-maintain by local proliferation rather than monocyte recruitment.[9–12] In mammals, TRMs are found in all organs with similar functions (i.e., scavenging of necrotic or apoptotic cells, invading pathogens, and maintaining homeostasis) and specific functions (i.e., participating in iron recycling, metabolism, synaptic information transfer, or cardiac conduction) depending on their anatomical location.[12,13]

During acute inflammation, recruitment of circulating monocytes triggered by LPS is a double-edged sword, which plays important roles in antimicrobial immune defense and tissue healing, but also contributes to the pathogenesis of inflammatory and degenerative diseases through promoting the inflammation and hindering the resolution.[14] However, unlike bone marrow-derived monocytes/macrophages (BMDMs), TRMs are able to conduct silent clearance of apoptotic cells with low expression of Toll-like receptor 9 (TLR9) and less TLR responsiveness to nucleic acids, which does not promote the inflammatory response.[15] Notably, recent evidence proved that

Received 15 July 2020; accepted 29 November 2020;
https://doi.org/10.1016/j.ymthe.2020.12.001.

Correspondence: Guo-Chang Fan, PhD, Department of Pharmacology and Systems Physiology, University of Cincinnati College of Medicine, 231 Albert Sabin Way, Cincinnati, OH 45267-0575, USA.
E-mail: fangg@ucmail.uc.edu
Correspondence: Xingjiang Mu, PhD, Department of Pharmacology and Systems Physiology, University of Cincinnati College of Medicine, 231 Albert Sabin Way, Cincinnati, OH 45267-0575, USA.
E-mail: muxingjiang@163.com

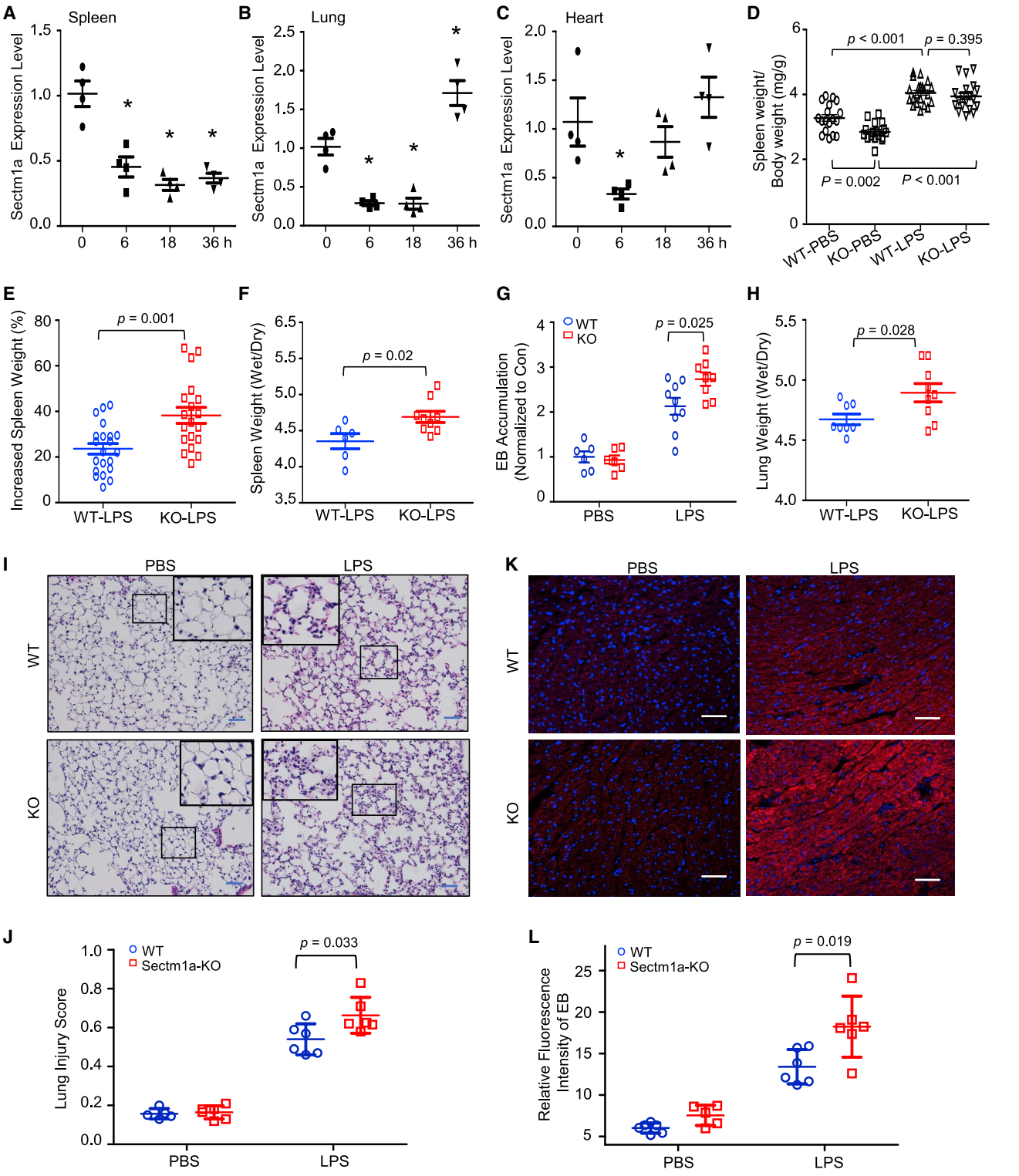

(legend on next page)

TRMs prevented neutrophil influx, neutrophil-mediated monocyte infiltration, and inflammatory damage through prostrating their membranes to cloaking the minor tissue damage.[16] Furthermore, TRMs are found to successively lose self-renewal capacity (the capability of proliferation) with age, leading to the reduction of their population in organs.[17–20] Although, as the first defense line, TRMs sit in the tissue and work silently without detrimental effects, there is still a heavy influx of inflammatory monocytes and neutrophils during acute inflammation. Herein, we hypothesized that there was a reduction in TRMs under acute inflammation, which generated demand for the recruitment of macrophages and triggered the infiltration of neutrophils and inflammatory monocytes. Therefore, upregulating the local proliferation of TRMs may contribute to stabling the TRM populations in tissues, preventing the detrimental infiltration of monocytes/neutrophils and favoring homeostasis/healing over further tissue damage caused by acute inflammation.

Mouse Sectm1a (secreted and transmembrane 1A) shares the greatest homology to human Sectm1[21–23] and has been characterized as an alternative CD7 ligand that is able to co-stimulate T cell proliferation and interleukin-2 (IL-2) release.[24,25] In mouse, Sectm1a also acted as a co-stimulator of T cells to enhance T cell proliferation and IL-2 production, but this action was implicated to work through binding to GITR (glucocorticoid-induced tumor necrosis factor receptor-related protein) rather than CD7.[23] Recently, Tsalik et al.[26] reported that expression levels of Sectm1 were higher in peripheral blood of sepsis survivors compared with non-survivors. However, to our knowledge, the functional role of Sectm1a has never been investigated in TRM biology.

In this study, we discovered that Sectm1a, as a novel GITR ligand, contributed to maintaining the self-renewal capacity of TRMs through boosting Th2 effector cells during endotoxemia. Furthermore, the administration of recombinant Sectm1a (rSectm1a) significantly attenuated LPS-induced reduction of TRMs and detrimental influx of inflammatory monocytes/neutrophils and improved the mouse survival following LPS injection. Hence elevation of Sectm1 levels could be a new therapeutic approach for inflammatory disease.

RESULTS

Loss of Sectm1a Aggravates Endotoxin-Induced Multi-organ Damage in Mice

To determine whether Sectm1a levels are altered in mice after LPS injection, we collected different organs at indicated time points. We found that LPS administration significantly downregulated Sectm1a expression levels in spleens (2.2-fold repression, $p = 0.004$), lungs (3.5-fold decrease, $p < 0.001$), and hearts (2.8-fold reduction, $p = 0.027$) at 6 h post-LPS injection (Figures 1A–1C). Sectm1a remained to be downregulated only in the spleen as late as 36 h post-LPS injection, whereas in the lung, Sectm1a had a 1.7-fold increase at 36 h post-LPS treatment compared with vehicle controls ($p = 0.012$). In addition, our immunofluorescence stain results also confirmed the downregulation of Sectm1a in the spleen ($p < 0.001$) and heart ($p < 0.001$) of LPS-treated mice (Figures S1A–S1D). Similarly, we found that sepsis patients had significantly lower levels of Sectm1 in the plasma compared with healthy donors (35.7 versus 132.2 ng/mL; $p = 0.033$) (Figure S1E). Taken together, these data suggest that the reduction of Sectm1a may contribute to the pathogenesis of acute inflammation. Given that Sectm1a is a secreted transmembrane protein, we therefore utilized a global Sectm1a-knockout (KO) mouse model to investigate its possible role in endotoxin-induced organ damages (Figure S2A). The loss of Sectm1a in KO mouse was confirmed in the spleen (Figure S2B) and heart (Figure S2C) by using the immunofluorescence staining technique. As shown in Figures S2D and S2E, there were no morphological abnormalities in KO mouse spleen and lung, compared with wild type (WT), at different ages. In addition, our complete blood count data did not present any significant difference between WT and KO mice at different ages (Table S1).

Spleen, the largest second lymphoid organ in human, plays important roles in immunity.[27] Loss of function of the spleen, either by splenectomy or infiltrative disease, is known to prominently increase the risk for severe infection and sepsis (five to six times higher).[28] Considering that Sectm1a is highly expressed in the spleen,[23] we then first determined whether loss of Sectm1a augmented splenomegaly or spleen edema in mice during acute inflammation. Interestingly, under basal PBS conditions, the ratio of spleen weight (SW) to body weight (BW) was significantly lower in Sectm1a-KO mice than that in WT mice ($p = 0.002$) (Figure 1D). However, the administration of LPS increased the ratio of SW/BW to a similar degree in both WT and KO mice at 24 h post-injection ($p = 0.395$) (Figure 1D). Hence further analysis showed that LPS actually caused higher increase of SW in KO mice than that in WT mice ($p = 0.001$) (Figure 1E). Accordingly, KO spleens possessed a remarkably higher ratio of wet weight/dry weight ($p = 0.02$) (Figure 1F) and more serious damage (evidenced by more enlargement of white pulp zone and larger presence of germinal centers) ($p < 0.001$) (Figures S2F and S2G) than WT spleens after LPS

Figure 1. Loss of Sectm1a Aggravates Endotoxin-Induced Multi-organ Damage in Mice

(A–C) After the administration of LPS (10 μg/g BW) to WT mice, the spleen (A), lung (B), and heart (C) were collected at indicated time points. Gene expression of Sectm1a in these tissues was determined by qRT-PCR (n = 4). (D–F) Sectm1a-KO mouse was generated as shown in Figure S2. At 24 h post-LPS (10 μg/g) or PBS injection, the spleen-to-body weight ratio (D) in WT and Sectm1a-KO mice was quantified, and the percentage increase (E) induced by LPS was calculated (n = 17–21). The ratio of spleen wet weight to dry weight (F) was also analyzed at the same time point post-LPS treatment (n = 6–9). (G) LPS-induced pulmonary vascular leakages were assessed by the extravasation of EB at 24 h post-LPS (10 μg/g) treatment. EB accumulation in different groups was normalized to control (n = 6–9). (H) Following 24 h of LPS (10 μg/g) treatment, ratios of lung wet weight to dry weight in WT and Sectm1a-KO mice were compared (n = 8–9). (I and J) Representative H&E staining images of lung sections at 24 h after PBS or LPS injection (I) are shown at ×200 original magnification. Scale bars, 50 μm. Lung injury scores (J) were assessed (n = 5–6). (K and L) Cardiovascular permeability was assessed by quantifying the extravasation of EB in the heart at 24 h post-treatment of PBS or LPS (10 μg/g). Blue represents DAPI, and red represents EB. Scale bars, 50 μm. n = 5–6. Data in all panels were pooled from at least two independent experiments. All results are presented as mean ± SEM and analyzed by Student's t test, one-way ANOVA, or two-way ANOVA.

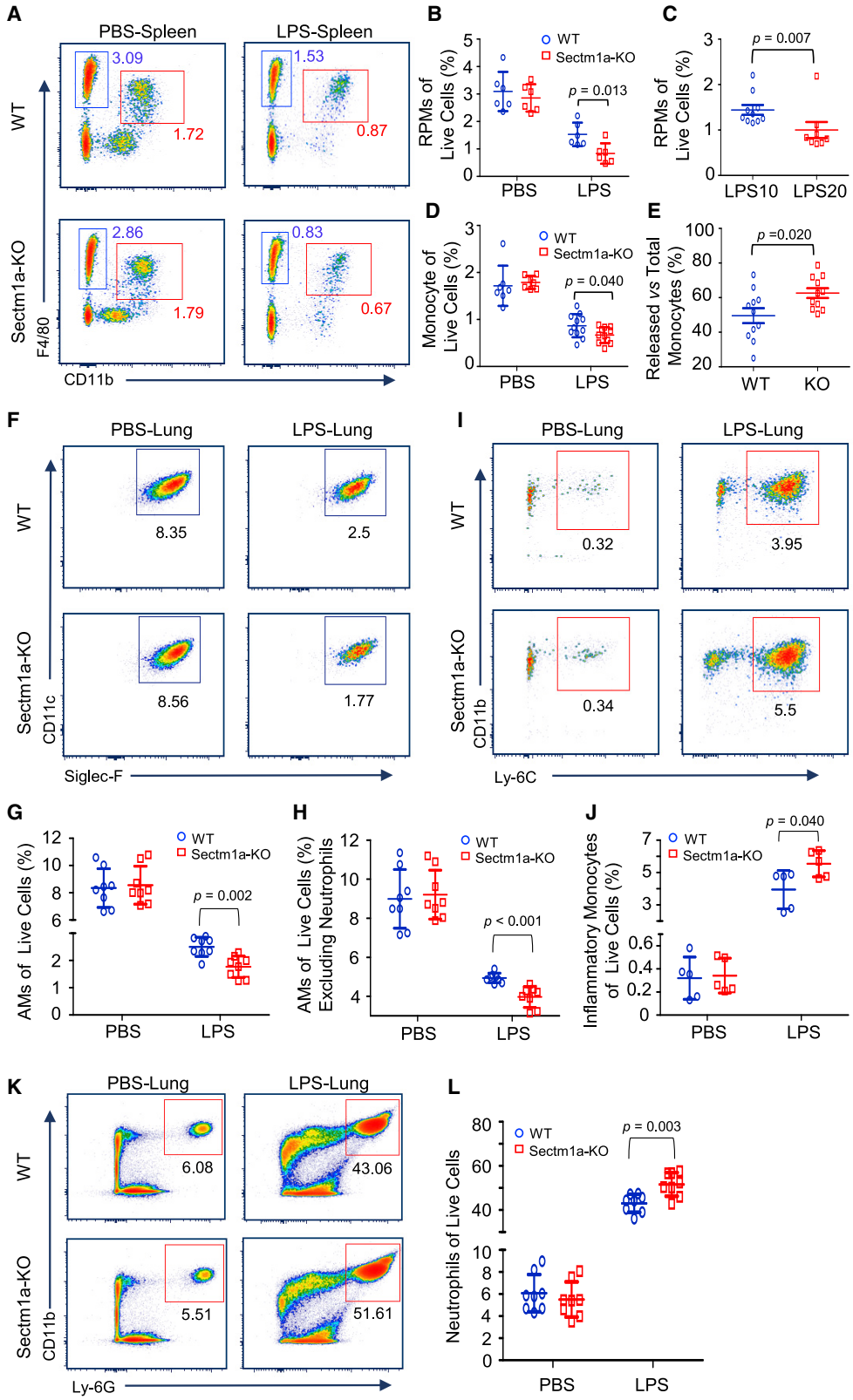

(legend on next page)

treatment, indicating that the loss of Sectm1a aggravated LPS-induced spleen edema and damage.

Next, we assessed lung injury characterized by pulmonary vascular hyperpermeability and neutrophilic inflammation in WT and Sectm1a-KO mice at 24 h post-LPS injection. As shown in Figure 1G, the Evans blue (EB) dye leakage in lung tissue was significantly increased in both WT and KO mice upon LPS treatment compared with vehicle controls, but such increase was more pronounced in KO lungs than WT controls ($p = 0.025$). Accordingly, similar effects and trends were observed in the wet weight/dry weight ratio of the lung ($p = 0.028$) (Figure 1H), indicating that LPS injection leads to more severe lung edema in KO mice than WT mice. At the same time point, we examined lung histology and found that both WT lungs and KO lungs exhibited normal structure under basal conditions. However, lung tissues collected from LPS-treated WT mice had extensive morphological damage and pathological abnormalities compared with PBS-WTs, including infiltration of neutrophils into the interstitium and alveolar spaces, increased hyaline membranes, increased alveolar wall thickness, and alveolar collapse (Figure 1I). Notably, the endotoxin-induced histopathological damage was aggravated in the Sectm1a-KO group (injury score, 0.66) compared with WT controls (injury score, 0.54) ($p = 0.033$) (Figure 1J). Altogether, these data indicate that loss of Sectm1a significantly exacerbates endotoxin-induced pathological lesions of lung.

Lastly, it is well recognized that a sepsis-induced systemic inflammatory response can directly induce cardiac vascular leakage and impair cardiac function;[29,30] thus, we assessed cardiovascular permeability in the heart of WT and KO mice with EB at 24 h post-LPS injection. As shown in Figures 1K and 1L, the red fluorescence intensity of EB extravasation was elevated by 2-fold in LPS-treated WT hearts, but this EB extravasation was further aggravated in LPS-treated KO hearts ($p = 0.019$). These results demonstrated that Sectm1a deficiency could exaggerate cardiovascular leakage in response to acute inflammation induced by endotoxin.

Ablation of Sectm1a Further Reduces the TRM Population in Mouse Spleen and Lung after LPS Injection

In the spleen, there are four sub-populations of macrophages, including red pulp macrophages (RPMs), marginal zone macrophages, marginal zone metallophilic macrophages, and tingible body macrophages, defined by anatomical compartments of red and white pulp regions. However, only RPMs are recognized as TRM, because they are seeded prenatally and maintained independently on substantial monocytic input.[31,32] In addition, as the largest distinct organ of the lymphatic system, the spleen also acts as a reservoir of inflammatory monocytes that rapidly deploy to damaged heart or lung during acute inflammation.[33,34] Once splenic monocytes localized at these sites, they are able to release inflammatory cytokines and promote the recruitment of neutrophils, which, in turn, exaggerate tissue damage in the heart and lung.[34–37] Therefore, in this study, we first utilized flow cytometry to analyze the population change of RPMs and splenic monocytes in both WT and Sectm1a-KO mice in response to acute inflammation. According to previous reports,[34,38] we characterized RPMs as CD45.2$^+$ Lin$^-$ CD11c$^-$ F4/80^{2+} CD11b$^{low/-}$ cells and splenic monocytes as CD45.2$^+$ Lin$^-$ CD11c$^-$ F4/80$^+$ CD11b^{2+} cells, and the gating strategy was shown in Figure S3A. Our analysis results showed that LPS (10 μg/g) treatment resulted in a loss of half of the RPM (blue gate) population in WT mice at 18 h post-injection (Figures 2A and 2B), and this reduction was dose dependent as shown in Figure 2C ($p = 0.007$). Interestingly, LPS exposure led to a further reduction (70.8%) of RPMs in Sectm1a-KO mice compared with WT mice (50.6%) ($p = 0.013$) (Figures 2A and 2B). As for splenic monocytes, fewer monocytes remained in KO spleens (0.67% of live cells) compared with that in WT spleens (0.87% of live cells) following LPS injection ($p = 0.04$) (Figure 2D). This means that the spleen in KO mice may release more monocytes into the circulating system compared with WT mice ($p = 0.02$) (Figure 2E).

In the lung, alveolar macrophages (AMs) are well recognized as resident macrophages and play a critical role in surfactant homeostasis and immune surveillance.[39] To investigate the population change of AMs at the earlier stage of acute inflammation, we collected all lung samples from mice at 18 h post-LPS treatment (10 μg/g) for flow cytometry analysis. The gating strategies for AMs (CD45.2$^+$ Ly-6G$^-$ CD3$^-$ CD19$^-$ MerTK$^+$ CD64$^+$ CD11c$^+$ Siglec-F$^+$ CD11b$^-$), infiltrated monocytes (CD45.2$^+$ Ly-6G$^-$ CD3$^-$ CD19$^-$ MerTK$^-$ Siglec-F$^-$ CD64$^+$ CD11b$^+$ Ly-6C$^+$), and neutrophils (CD45.2$^+$ Ly-6G$^+$ CD11b$^+$ Ly-6C$^+$) were shown in Figure S3B. We observed that the AM population (of live cells) dropped from 8.35% (PBS control) to 2.5% (LPS-treated) in WT mice (Figures 2F and 2G), However,

Figure 2. Sectm1a Deficiency Further Diminishes Tissue-Resident Macrophages in the Spleen and Lung after LPS Injection

The whole spleen and lung tissues were collected from WT and Sectm1a-KO mice at 18 h post-PBS or LPS (10 or 20 μg/g) injection and subjected to flow cytometry analyses. (A) Representative flow cytometry plots of red pulp macrophages (CD45.2$^+$ Lin$^-$ CD11c$^-$ F4/80^{2+} CD11b$^{low/-}$ cells, blue gate) and splenic monocyte (CD45.2$^+$ Lin$^-$ CD11c$^-$ F4/80$^+$ CD11b^{2+} cells, red gate) following PBS or LPS (10 μg/g) treatment. Gating strategy is shown in Figure S3A. (B) Percentages of RPM population in WT and KO spleen were summarized following PBS or LPS treatment (n = 6). (C) The percentage change of the RPM population in the spleen of WT mice in response to different doses (10 μg/g, 20 μg/g) of LPS (n = 8–10). (D) Calculation of the percentage of splenic monocytes in WT and Sectm1a-KO mice after PBS or LPS (10 μg/g) treatment (n = 7–11). (E) Quantification percentages of released monocytes in WT and KO mice with the formula: Percentage of released monocytes = [(percentage of monocytes in PBS group) − (percentage of monocytes remaining in LPS group)]/(percentage of monocytes in PBS group) (n = 11). (F–H) Representative flow cytometry plots of AMs (F) (CD45.2$^+$ Ly-6G$^-$ CD3$^-$ CD19$^-$ MerTK$^+$ CD64$^+$ CD11c$^+$ Siglec-F$^+$ CD11b$^-$) in the lung of WT and Sectm1a-KO mice after PBS or LPS injection. Gating strategy was shown in Figure S3B. Percentages of AMs in total live cells (G) and percentages of AMs in live cells excluding neutrophils (H) were quantified (n = 8). (I and J) Representative flow cytometry plots (I) of inflammatory monocytes (CD45.2$^+$ Ly-6G$^-$ CD3$^-$ CD19$^-$ MerTK$^-$ Siglec-F$^-$ CD64$^+$ CD11b$^+$ Ly-6C$^+$) in the lung following PBS or LPS administration. Percentages of infiltrated inflammatory monocytes in total live cells (J) are shown (n = 5). (K) Flow cytometry showing the infiltration of neutrophil (CD45.2$^+$ Ly-6G$^+$ CD11b$^+$ Ly-6C$^+$) in the lung after LPS injection. (L) Percentages of infiltrated neutrophils in total live cells (n = 8).

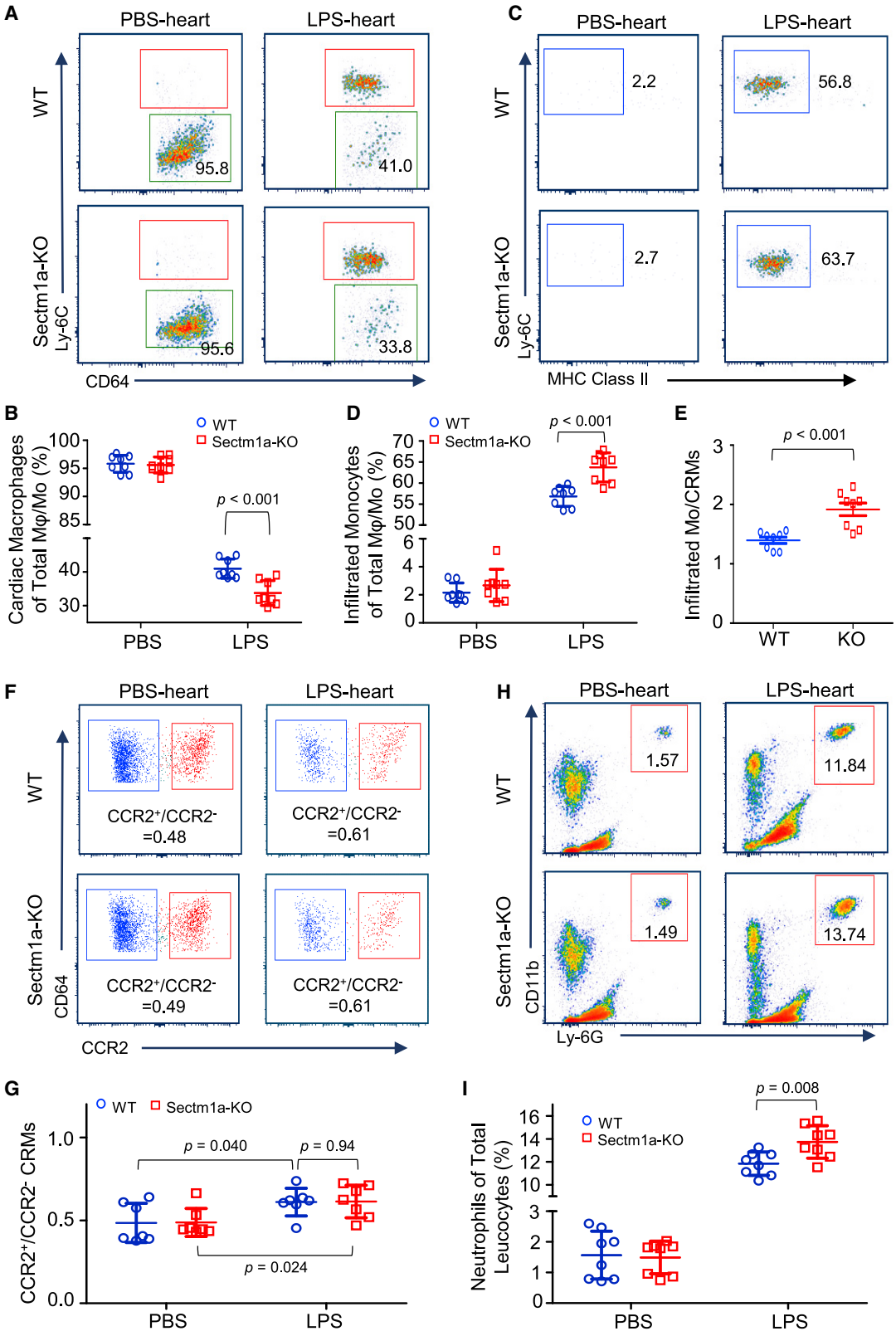

(legend on next page)

LPS-triggered reduction of AMs was more pronounced in Sectm1a-KO lungs, which was 1.4-fold less than that in WT lungs ($p = 0.002$) (Figures 2F and 2G). Given that LPS-triggered recruitment of a high amount of neutrophils also contributes to the drop of AM percentage in live cells, we then excluded neutrophils from live cells and re-calculated the percentage of AMs (of live cells). As shown in Figure 2H, our re-analysis results also confirmed that Sectm1a deficiency resulted in further decline of the AM population in response to acute inflammation ($p < 0.001$). In parallel, we found that the recruitment of inflammatory monocytes and neutrophils was further increased by 40% ($p = 0.04$) (Figures 2I and 2J) and 20% ($p = 0.003$) (Figures 2K and 2L), respectively, in LPS-treated KO lungs compared with those in LPS-treated WTs.

Loss of Sectm1a Exacerbates LPS-Induced Reduction of Cardiac-Resident Macrophages (CRMs) in the Heart

In the heart, TRMs were recently characterized as CD45.2$^+$ Ly-6G$^-$ F4/80$^+$ CD64$^+$ CD11b$^+$ Ly-6C$^-$ and play important roles in promoting coronary development, promoting cardiac regeneration, facilitating electrical conduction, and protecting cardiac functions.[40–42] However, whether the CRM population is affected by endotoxin remains unknown. Herein, we determined the CRM population change following LPS injection and found that the percentage of CRMs (gating strategy as shown in Figure S3C) in the total macrophage/monocyte population was decreased by more than half in WT mice at 18 h post-LPS injection (Figures 3A and 3B). Notably, LPS caused further reduction of CRMs in Sectm1a-KO mice ($p < 0.001$) (Figures 3A and 3B). Similar to what we observed in the lung, the percentages of cardiac inflammatory monocytes (CD45.2$^+$ Ly-6G$^-$ F4/80$^+$ CD64$^+$ CD11b$^+$ Ly-6C$^+$ MHCII$^-$) were respectively increased to 56.8% in WT mice and 63.7% in KO mice after LPS challenge ($p < 0.001$) (Figures 3C and 3D). Further analysis revealed that the ratio of inflammatory monocytes to CRMs was much higher in LPS-KO mice than LPS-WTs, indicating more influx of inflammatory monocytes to KO hearts ($p < 0.001$) (Figure 3E). Similar to human hearts, mouse CRMs can also be partitioned into two distinct subsets depending on the expression of CCR2. In this study, our flow cytometry results revealed that LPS treatment significantly increased the ratio of CCR2$^+$ to CCR2$^-$ in both WT and KO hearts, but there was no difference between the two mouse groups in this ratio before or after LPS treatment (Figures 3F and 3G). However, Sectm1a depletion significantly exaggerated LPS-induced infiltration of neutrophils into the heart, compared with WTs ($p = 0.008$) (Figures 3H and 3I).

Sectm1a Deficiency Exacerbates Endotoxin-Induced Proliferation Suppression in TRMs

To understand why the loss of Sectm1a augments LPS-induced reduction of TRMs, we first examined apoptosis/necrosis in mouse RPMs and AMs at 16 h post-LPS injection. Our flow cytometry results revealed that there were not any differences in the degree of apoptosis/necrosis between WT-RPMs and KO-RPMs in response to endotoxin treatment (Figures S4A–S4C). A similar degree of apoptosis/necrosis was also observed between WT-AMs and KO-AMs after endotoxin challenge (Figures S4D–S4F). These results exclude the contribution of cell mortality to the further reduction of TRMs in KO mice during acute inflammation compared with WT mice. Therefore, we speculated that such Sectm1a deficiency-increased reduction of TRMs may be ascribed to the decreased local proliferation. Using intracellular staining flow cytometry, we analyzed the percentage of Ki-67$^+$ (a widely used cellular marker for proliferation) cells in TRMs before and after LPS treatment. As shown in Figures 4A and 4B, proportions of Ki-67$^+$ RPMs were respectively dropped by 1.6-fold and 2.4-fold in WT mice and KO mice at 12 h post-LPS injection, and the proportion of Ki-67$^+$ RPMs in KO mice was 2-fold less than that in WT mice after LPS treatment ($p < 0.001$). In addition, our results also revealed that Ki-67$^+$ RPMs were reduced significantly in the Sectm1a-KO mice compared with WT mice under PBS treatment (Figure 4B). This reduction may be ascribed to the abundance of Sectm1a and T cells in the mouse spleen. Next, these flow cytometry results were further confirmed by co-immunofluorescence staining of spleens with antibodies for F4/80 and Ki-67 (Figure 4C).

Similarly, we found that the proliferation of lung-resident macrophages (AMs) was also significantly inhibited in both WT and KO mice upon LPS challenge, but KO mice presented a larger degree of reduction ($p = 0.017$), as evidenced by a 2-fold decrease of Ki-67$^+$ AMs in WT mice versus a 3-fold decrease in KO mice at 12 h post-LPS treatment (Figures 4D and 4E). Meanwhile, the mean fluorescence intensity (MFI) of Ki-67 was significantly lower in Ki-67$^+$ AMs from LPS-treated KO mice ($p = 0.013$) (Figure 4F). With regard to CRMs, the fractions of Ki-67$^+$ CRMs ($p = 0.001$) and their MFI ($p = 0.01$) were also decreased to a significantly lower degree in Sectm1a-KO mice compared with that in WT mice after LPS stimulation (Figures 4G–4I). In addition, our further analysis revealed that although the local proliferations of CCR2$^-$ ($p < 0.001$) and CCR2$^+$ ($p = 0.023$) CRMs were both significantly downregulated by LPS administration,

Figure 3. Loss of Sectm1a Exacerbates LPS-Induced Reduction of Cardiac-Resident Macrophages (CRMs) in the Heart

The whole hearts were collected from WT and Sectm1a-KO mice at 18 h after PBS or LPS (10 μg/g) injection and were subjected to flow cytometry analyses. (A and B) Representative flow cytometry plots of CRM (CD45.2$^+$ Ly-6G$^-$ F4/80$^+$ CD64$^+$ CD11b$^+$ Ly-6C$^-$) (green gate) in WT and Sectm1a-KO mice in response to endotoxin (A). Gating strategy is shown in Figure S3C. Percentages of CRM (B) in the total macrophage and monocyte population (n = 8). (C–E) Representative flow cytometry plots of inflammatory monocytes (CD45.2$^+$ Ly-6G$^-$ F4/80$^+$ CD64$^+$ CD11b$^+$ Ly-6C$^+$ MHCII$^-$) in the heart following LPS administration (C). Percentages of infiltrated inflammatory monocytes (D) in the total macrophage and monocyte population (n = 8). Comparative analysis of the ratio of inflammatory monocytes to CRM (E) in WT and Sectm1a-KO mice after LPS injection (n = 8). (F and G) Representative flow cytometry plots (F) and ratios of CCR2$^+$ to CCR2$^-$ CRMs (G) in WT and Sectm1a-KO mice after PBS or LPS injection (n = 7). Gating strategy is shown in Figure S3C. (H and I) Flow cytometry showing the infiltration of neutrophils (CD45.2$^+$ CD11b$^+$ Ly-6G$^+$ Ly-6C$^+$) in the heart (H) after PBS or LPS injection. Percentages of infiltrated neutrophils in total leukocytes of heart (n = 8) (I). Data in all panels were pooled from at least two independent experiments. All results are presented as mean ± SEM and analyzed by Student's t test or one-way ANOVA.

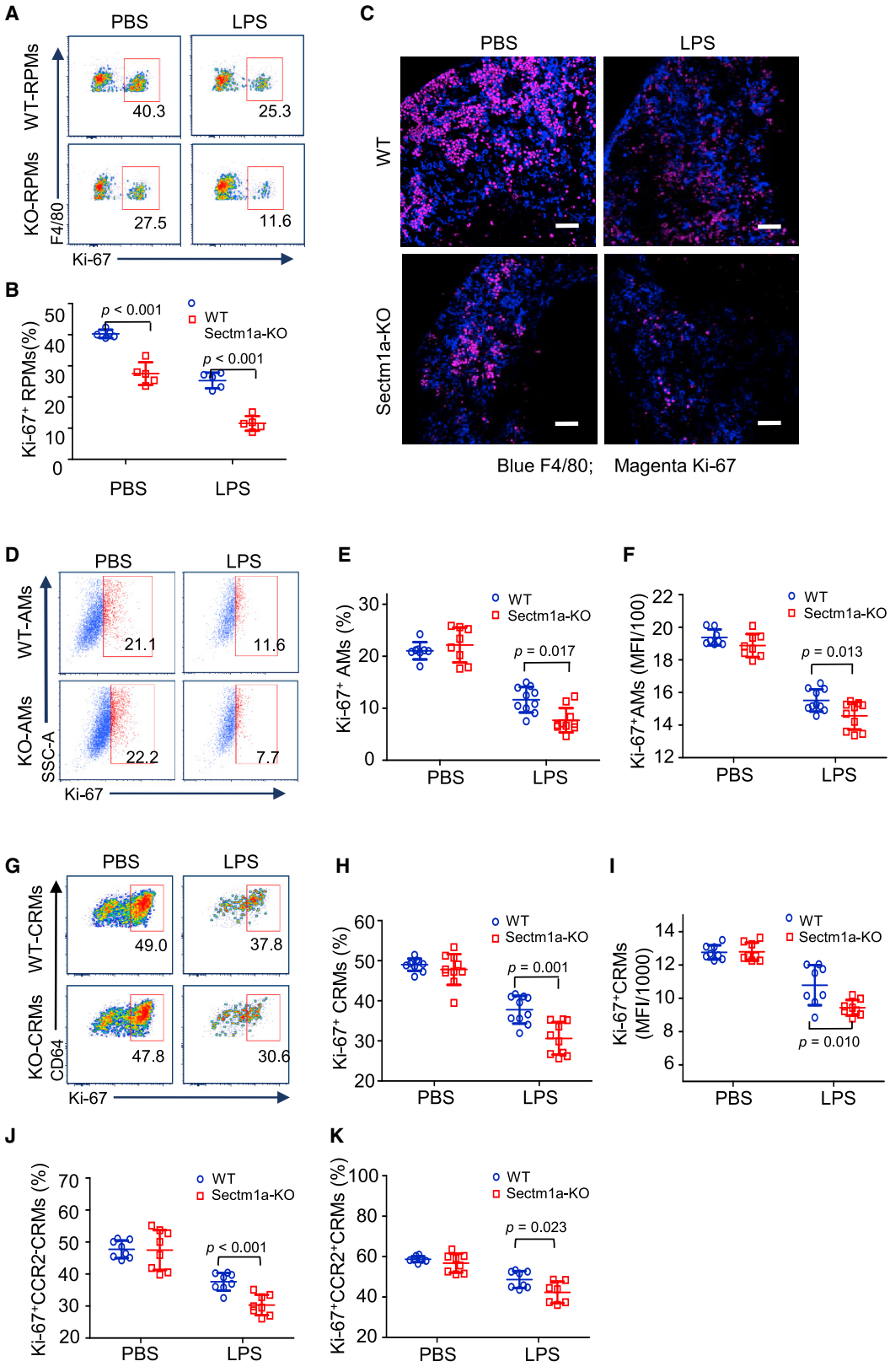

(legend on next page)

more reductions were observed in Sectm1a-KO mice compared with WTs (Figures 4J and 4K). Interestingly, Ki-67$^+$ CCR2$^-$ CRMs were decreased more than Ki-67$^+$ CCR2$^+$ CRMs after LPS injection in both WT and KO mice, which may explain the increased ratio of CCR2$^+$ to CCR2$^-$ in the CRM population. Together, these data suggest that Sectm1a could be essential for local proliferation of TRMs and contribute to the maintenance of their population in multiple organs upon endotoxin stress.

rSectm1a Promotes the Proliferation of TRMs through Boosting the Expansion of T Helper (Th) Cells

To further determine the effect of Sectm1a on TRM proliferation, we isolated RPMs from spleens of WT or KO mice as described in our recent publication.[43] Then RPMs were labeled with CellTracker fluorescence reagent and grown for 48 h to monitor cell proliferation. Unexpectedly, the fluorescence intensity showed no difference between WT-RPMs and Sectm1a-deficient RPMs (Figure S5A), indicating that ablation of Sectm1a in RPMs has no effect on their proliferation. In addition, treatment of WT-RPMs with rSectm1a did not affect RPM proliferation (Figure S5B). However, in our positive control group (using IL-4 as a stimulator of macrophage growth),[44,45] there was remarkably higher fluorescence intensity compared with the PBS-treated group ($p < 0.05$) (Figure S5B). These results were further confirmed by the staining of RPMs with 5-ethynyl-2′-deoxyuridine (EdU) (cell proliferation marker), as evidenced by a similar proliferation rate in RPMs isolated from either WT or Sectm1a KO mice, regardless of the addition of rSectm1a (Figures S5C and S5D). Taken together, all these data indicate that Sectm1a could not directly regulate TRM proliferation. Hence we speculated that Sectm1a might affect other cell types, which, in turn, crosstalk with TRMs and impact their proliferation.

Given that Sectm1 and Sectm1a were both reported to be able to co-stimulate T cell proliferation and IL-2 release,[23–25] we thus hypothesized that Sectm1a might also promote the differentiation of Th2 and the release of IL-4, which, in turn, stimulated the proliferation of TRMs. To this end, we co-cultured naive CD4 T cells with RPMs. As shown in Figure 5A, RPMs were seeded on the coverslip of the lower chamber at the same density, and naive CD4 T cells were isolated from mice and cultured on the upper insert, which was coated with rSectm1a (2 μg/mL) or IgG2a (1.25 μg/mL). At the same time, Dynabeads covalently coupled to anti-CD3 and anti-CD28 antibodies were added to stimulate CD4 naive T cells. After 4 days of stimulation, half of the cells were treated with 200 ng/mL LPS for 24 h. Then supernatants were collected to measure cytokine levels, and RPMs were stained with F4/80 (red) and EdU (green). Meanwhile, to assess the effect of rSectm1a on the differentiation of naive CD4 T cells, we carried out intracellular cytokine assays for interferon (IFN)-γ and IL-4 following PMA and ionomycin stimulation. We observed that RPM populations in the rSectm1a-treated group were significantly increased by 2.3-fold ($p < 0.001$) in the absence of LPS and 2.5-fold ($p < 0.001$) in the presence of LPS (Figures 5B and 5C), respectively, compared with their isotype controls. It is important to note here that the application of LPS led to 50% reduction in the RPM population, which is consistent with our *in vivo* experiment results (Figures 2A–2C). Accordingly, the percentage of EdU$^+$ RPMs in the rSectm1a-treated group was around two times higher than that in isotype control under LPS exposure ($p < 0.001$) (Figures 5D and 5E), indicating a higher proliferating rate induced by rSectm1a treatment. Meanwhile, our flow cytometry results showed that rSectm1a dramatically elevated the percentage of IL-4-producing CD4 T cells by 18-fold in the absence of LPS and 15-fold in the presence of LPS *in vitro* compared with isotype control groups (Figure 5F). In line with previous reports about rSectm1a-mediated Th1 polarization, we also observed that the number of IFN-γ-producing CD4 T cells was significantly increased by 10-fold in the absence of LPS and 2-fold in the presence of LPS *in vitro* after rSectm1a treatment (Figure 5F). Next, we compared the differentiation of Th1 and Th2 cells *in vivo* between WT and KO mice at 12 h post-LPS treatment. As shown in Figures 5G–5I, Sectm1a depletion significantly reduced Th2 (IL-4$^+$ CD4 cells) ($p = 0.007$) and Th1 (IFN-γ$^+$ CD4 cells) ($p < 0.001$) populations in the spleen of LPS-treated mice, coinciding with our *in vitro* results. As for Th2-associated cytokines (i.e., IL-4 and IL-5), we found that both IL-4 ($p = 0.04$) and IL-5 ($p = 0.049$) levels were significantly higher in the co-culture supernatants collected from the rSectm1a-treated group than those collected from isotype controls (Figures 5J and 5K). Furthermore, levels of GM-CSF (granulocyte-macrophage colony stimulating factor), another stimulator of TRM proliferation, were also remarkably increased by rSectm1a treatment ($p < 0.001$) (Figure 5L). Consistent with these *in vitro* findings, serum levels of IL-4 ($p = 0.031$), GM-CSF ($p = 0.025$), and macrophage colony-stimulating factor (M-CSF; $p = 0.008$) were significantly lower in Sectm1a-KO mice than WT mice following LPS treatment (Figures 5M–5O). Taken together, our results demonstrate that Sectm1a positively promotes RPM proliferation through driving Th1 and Th2 polarization and relevant cytokine release.

GITR Is Critical for the Sectm1a-Mediated Regulatory Effect on the Activation of Th Cells

Although Howie et al.[23] identified GITR as a Sectm1a receptor on T cells *in vitro*, it remains unclear whether Sectm1a-mediated effects on primary Th cells are dependent on GITR *in vivo*. Therefore, we conducted the following experiments with GITR-KO mice.

Figure 4. Sectm1a Deficiency Exacerbates Endotoxin-Induced Proliferation Suppression in Tissue-Resident Macrophages

The spleen, lung, and heart in WT and Sectm1a-KO mice were collected and subjected to flow cytometry analysis at 16 h after PBS or LPS (10 μg/g) administration. (A, D, and G) Representative flow cytometry plots showing Ki-67$^+$ RPMs (A), AMs (D), and CRMs (G), respectively. (B, E, and H) Percentages of Ki-67$^+$ RPMs (B), AMs (E), and CRMs (H) after PBS or LPS injection (n = 5–10). (C) Immunofluorescent staining of spleen sections with F4/80 (blue) and Ki-67 (magenta) at 16 h after PBS or LPS treatment. Scale bar: 50 μm. (F and I) Quantification of mean fluorescence intensity (MFI) in Ki-67$^+$ AMs (F) and CRMs (I) (n = 8–10). (J and K) Percentages of Ki-67$^+$ cell population in CCR2$^-$ (J) and CCR2$^+$ (K) CRMs following PBS or LPS injection (n = 7–8). Data in all panels were pooled from at least two independent experiments. All results are presented as mean ± SEM and analyzed by Student's t test or one-way ANOVA.

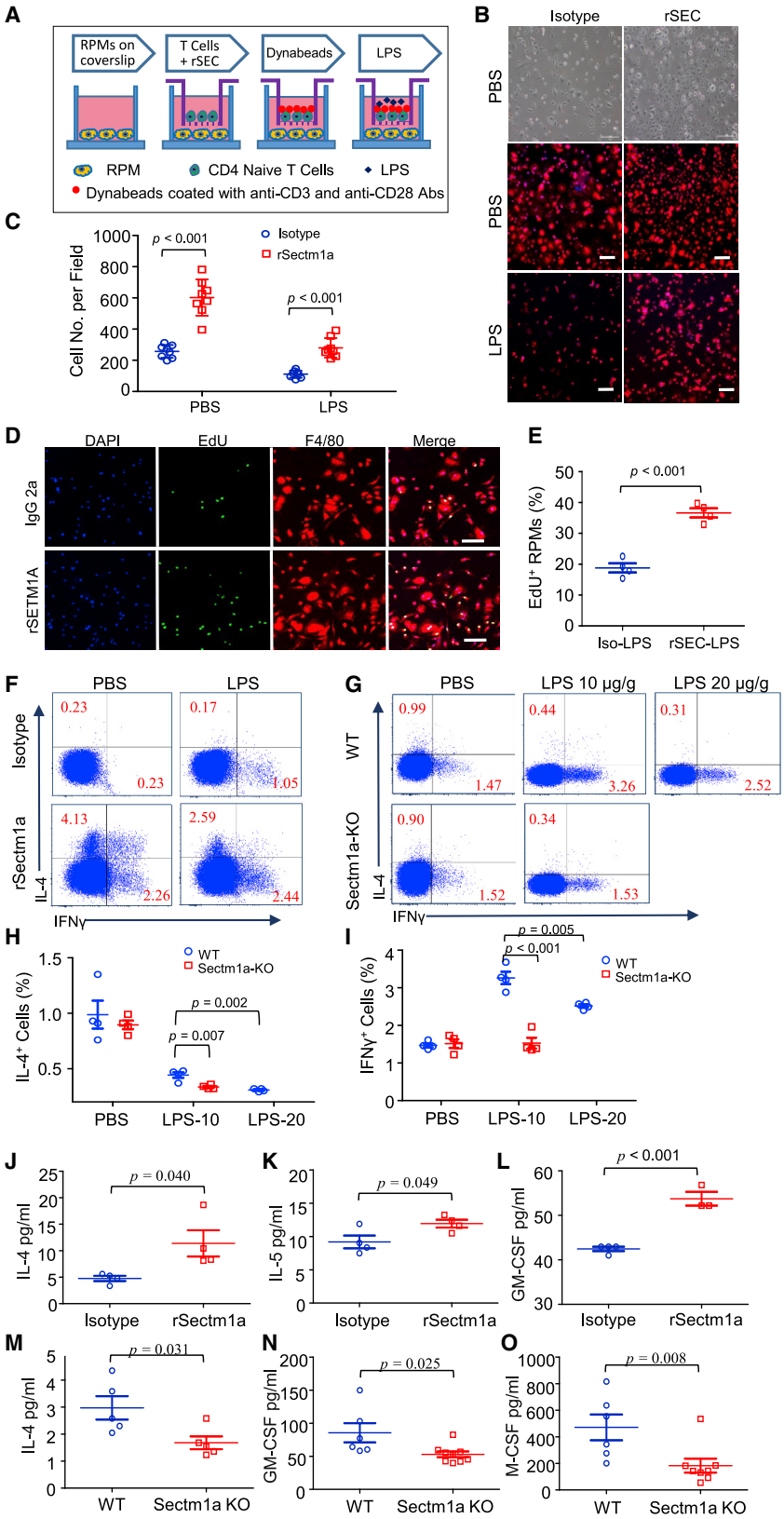

Figure 5. rSectm1a Promotes the Proliferation of Tissue-Resident Macrophages through Boosting the Expansion of T Helper Cells

(A) RPM and naive CD4 T cell co-culture experiment design. (B) Representative bright-field image and immunofluorescence stain image of RPMs after co-culturing with IgG2a-treated or rSectm1a-treated naive CD4 T cells in the absence or presence of LPS (red represents F4/80; blue represents DAPI). Scale bars, 100 μm. (C) The proliferation of RPMs was assessed by counting cell numbers per microscopic field. All determinations were performed for at least three independent experiments (n = 8). (D and E) Representative immunofluorescence stain images (D) and quantification (E) of EdU-positive RPMs under co-culture condition following different treatments. Results are shown as means ± SEM of four independent experiments, and 200–300 cells were analyzed per experiment (n = 4). Scale bars, 100 μm. (F) Percentages of $CD4^+$ IFN-γ^+ T cell (Th1) and $CD4^+$ IL-4^+ T cell (Th2) after co-culture with RPMs in the absence or presence of LPS were shown in representative dot plots. (G–I) The intracellular cytokine assays for IFN-γ and IL-4 in CD4 T cell isolated from the spleen of WT or KO mice after LPS injection (G). (H and I) Percentages of $CD4^+$ IL-4^+ T cell (Th2) (H) and $CD4^+$ IFN-γ^+ T cell (Th1) (I) *in vivo* in response to endotoxin treatment (n = 4). (J–L) After co-culture, cytokine levels of IL-4 (J), IL-5 (K), and GM-CSF (L) in cell culture supernatants were measured by using Luminex technology (n = 3–4). (M–O) At 12 h post-LPS (10 μg/g) injection, cytokine levels of IL-4 (M), GM-CSF (N), and M-CSF (O) in sera were determined in WT and Sectm1a KO mice by using Luminex. (n = 5–8). All results are presented as mean ± SEM and analyzed by Student's t test or one-way ANOVA.

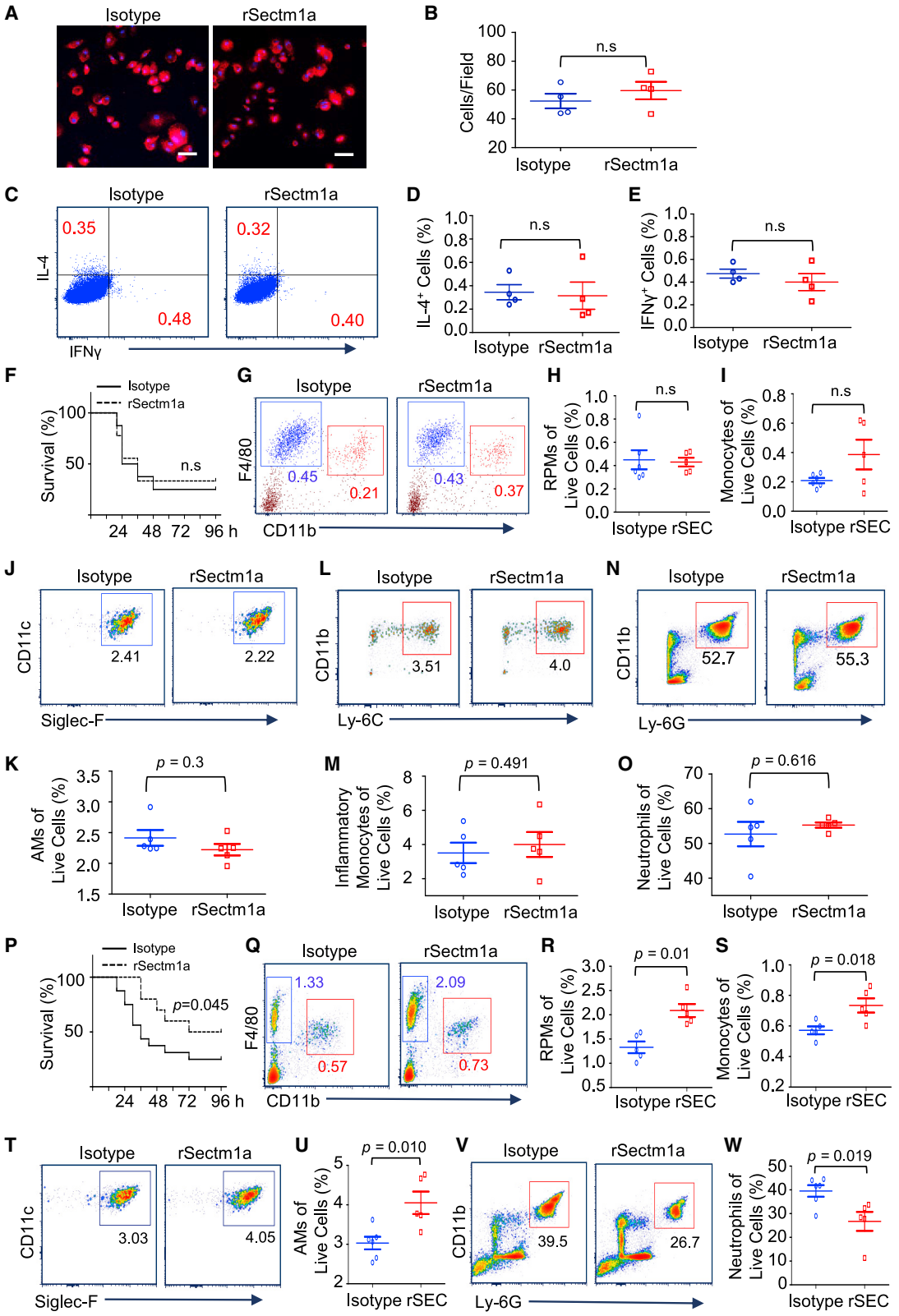

(legend on next page)

First, we isolated naive CD4 T cells from GITR-KO mice and co-cultured them with RPMs from WT mice following the same protocol used above (Figure 5A). After 6 days of co-culture, we found that rSectm1a treatment did not significantly increase the RPM population (Figures 6A and 6B). As expected, using naive CD4 T cells isolated from GITR-KO mice, rSectm1a treatment also failed to stimulate the differentiation of either Th1 or Th2 (Figures 6C–6E). In addition, the administration of rSectm1a to GITR-KO mice displayed no effects on LPS-induced animal mortality (Figure 6F). Accordingly, rSectm1a treatment did not attenuate the decrease of either RPMs or splenic monocytes in GITR-KO mice during acute inflammation (Figures 6G–6I). Similarly, rSectm1a injection also failed to increase the AMs population (Figures 6J and 6K) and reduce the infiltration of inflammatory monocytes (Figures 6L and 6M) and neutrophils (Figures 6N and 6O) in the lung of LPS-treated GITR-KO mice. However, the administration of rSectm1a to WT mice significantly improved the animal survival in response to endotoxin challenge (Figure 6P). In addition, rSectm1a treatment significantly increased the RPM population ($p = 0.01$) and attenuated the reduction of splenic monocytes ($p = 0.018$) in LPS-treated WT mice (Figures 6Q–6S). As expected, the injection of rSectm1a also significantly enhanced the AM population ($p = 0.01$) (Figures 6T and 6U) and reduced the infiltration of neutrophils ($p = 0.019$) (Figures 6V and 6W) in the lung of WT mice during acute inflammation. In addition, the administration of rSectm1a did not cause any morphological change in mouse spleen and lung according to our H&E staining results (Figure S6A). Our complete blood count data did not present any significant difference after the administration of rSectm1a (Table S2). Furthermore, we also tried to determine the cytokine (TNF-α and IL-6) levels in the serum of IgG2a-treated and rSectm1a-treated mice at 24 h post-treatment. As expected, both of them were undetectable. These results indicate that the administration of rSectm1a is not toxic for mice. Taken together, both our *in vitro* and *in vivo* results suggest that GITR is pivotal for the Sectm1a-mediated impact on the expansion of Th cells and TRMs.

TRMs Are Essential for Maintaining Local Vascular Integrity during Acute Inflammation

Lastly, to understand why the reduction of TRMs was associated with the recruitment of inflammatory leukocytes into multiple organs during endotoxemia, we pre-depleted TRMs with clodronate liposome and determined its consequential effect on the LPS-induced vascular leakage, a major contributor to sepsis-caused organ failure. After 3-day application of clodronate liposome, our flow cytometric analysis confirmed that TRMs in spleens and lungs were successfully diminished (Figures 7A and 7B). At 24 h post-LPS injection, we observed that the ratio of spleen wet weight/dry weight in macrophage pre-depleted mice was significantly higher than that in control mice ($p = 0.013$) (Figure 7C). In addition, LPS administration also resulted in more EB leakage ($p = 0.038$) and morphological damage ($p = 0.026$) in lungs of clodronate-treated groups compared with controls (Figures 7D–7F). Similarly, pre-depletion of macrophages also significantly increased cardiovascular permeability in response to endotoxin ($p = 0.032$) (Figures 7G and 7H). In line with our *in vivo* findings, our *in vitro* results showed that the presence of RPMs significantly attenuated the thrombin-induced endothelial barrier disruption ($p = 0.003$) (Figure 7I). Mechanistically, we found that the RPM conditioned medium significantly upregulated mRNA levels of ZO-1 (tight-junction proteins) ($p = 0.012$), VE-cadherin (adherens-junction protein) ($p = 0.01$), and occludin ($p = 0.003$) in endothelial cells (ECs) (Figures 7J–7L), and our western blot results also confirmed the upregulation of ZO-1 and VE-cadherin (Figure S6B). Moreover, our confocal microscopy examination clearly presented a more dense distribution of tight-junction protein between ECs in the presence of RPM medium (Figure 7M). Accordingly, under thrombin or PMA stimulation, less fragmentation and depletion of ZO-1 were observed between ECs cultured in RPM-conditioned medium compared with that cultured in normal medium (Figure 7M), suggesting that RPM-conditioned medium helped to maintain ZO-1 dense distribution and linear pattern between ECs. Taken together, our results indicate the important role of TRMs in stabilizing the local vascular integrity.

Figure 6. GITR Is Critical for a Sectm1a-Mediated Regulatory Effect on the Activation of T Helper Cells

(A–E) Following the same co-culture design in Figure 5A, RPMs isolated from WT mice were co-cultured with naive CD4 T cells isolated from GITR-KO mice. (A) Representative immunofluorescence stain image of RPMs after treatment (red represents F4/80, and blue represents DAPI). Scale bars, 50 μm. (B) The proliferation of RPMs was assessed by counting cell numbers per microscopic field. All determinations were performed for at least three independent experiments (n = 4). (C) Representative flow cytometry dot plots of $CD4^+$ IFN-γ^+ T cells ($GITR^{-/-}$) and $CD4^+$ IL-4^+ T cells ($GITR^{-/-}$) after co-culture with RPMs in the absence or presence of rSectm1a. (D and E) Percentages of $CD4^+$ IL-4^+ T cells ($GITR^{-/-}$) (D) and $CD4^+$ IFN-γ^+ T cells ($GITR^{-/-}$) (E) after co-culture (n = 4). (F–O) After intraperitoneal (i.p.) injection with LPS (10 μg/g), GITR-KO mice were immediately injected intravenously (i.v.) with IgG2a (125 μg/kg) (isotype) or rSectm1a (200 μg/kg). (F) Mouse survival was monitored for up to 96 h post-LPS treatment (n = 8–9). (G–O) At 18 h after last treatments, spleen and lung tissues were collected and subjected to flow cytometry experiments. (G–I) Representative flow cytometry plots (G) of RPMs (blue gate) and splenic monocytes (red gate) in GITR-KO mice with rSectm1a treatment or IgG2a treatment. The percentage of RPMs (H) and monocytes (I) in the live cells were calculated (n = 5–6). (J and K) Representative flow cytometry plots (J) and quantification (K) of AMs in the lung after different treatments. (L and M) Representative flow cytometry plots (L) and quantification (M) of inflammatory monocytes in the lung. (N and O) Representative flow cytometry plots (N) and quantification (O) of neutrophils in the lung. (P) After i.p. injection with LPS (15 μg/g), WT mice were immediately injected i.v. with IgG2a (125 μg/kg) (isotype) or rSectm1a (200 μg/kg) and monitored for survival up to 96 h post-LPS treatment (n = 10–16). (Q–W) WT mice were immediately injected i.v. with IgG2a (125 μg/kg) (isotype) or rSectm1a (200 μg/kg) following LPS (10 μg/g) i.p. injection. At 18 h after last treatments, the spleen and lung tissues were collected and subjected to flow cytometry experiments. (Q–S) Representative flow cytometry plots (Q) of RPMs (blue gate) and splenic monocyte (red gate) in WT mice with rSectm1a (or isotype) treatments and quantification of RPMs (R) and splenic monocytes (S) (n = 5). (T and U) Representative flow cytometry plots (T) and quantification of AMs (U) in the lung after different treatments (n = 5–6). (V and W) Representative flow cytometry plots (V) and quantification of neutrophils (W) in the lung (n = 5–6). Data in all panels were pooled from at least two independent experiments. All results are presented as mean ± SEM and analyzed by Mann-Whitney test, Student's t test, or one-way ANOVA.

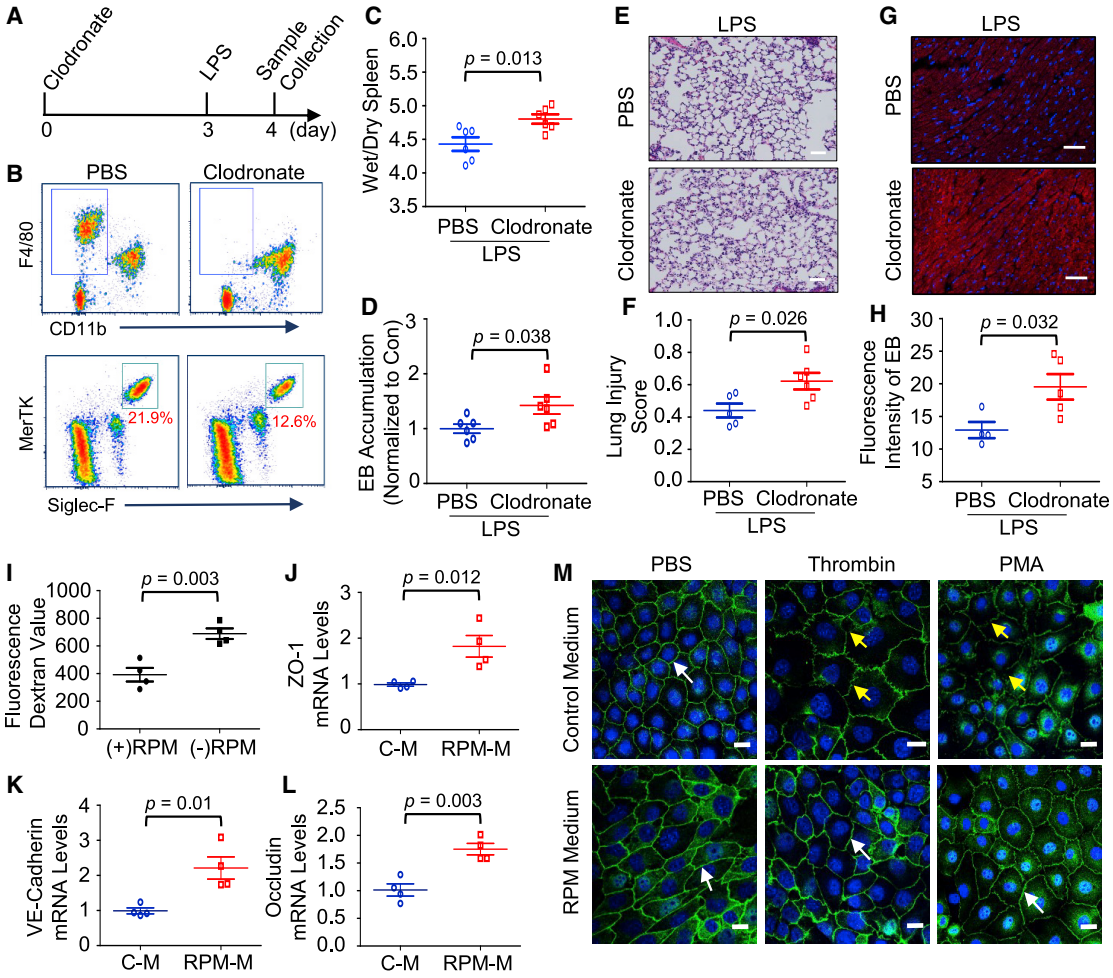

Figure 7. Tissue-Resident Macrophages Are Essential for Maintaining Local Vascular Integrity during Endotoxemia

(A) Graphic illustration of mouse treatment scheme. To pre-deplete tissue-resident macrophages, we injected (i.v.) WT mice with clodronate-liposome (200 μL, clodronate 5 mg/mL). The control mice received vehicle-liposome (200 μL, no clodronate). After 3 days, mice were injected (i.p.) with LPS (5 μg/g). At 24 h after LPS injection, the spleen, lung, and heart were collected for the following experiments. (B) Representative flow cytometry plots showing the reduction of RPMs in the spleen (upper plot) and AMs in the lung (lower plot) on day 3 after clodronate liposome treatment. (C) The ratio of spleen wet weight to dry weight in control and macrophage pre-depleted mice was measured at 24 h after LPS treatment (n = 6). (D) Meanwhile, LPS-induced pulmonary vascular leakages were assessed by the extravasation of EB (n = 6). (E) Representative H&E staining images of lungs at 24 h after LPS injection were shown at ×200 original magnification; scale bars, 50 μm. (F) The lung injury scores were calculated (n = 5–6). (G and H) Cardiovascular permeability was assessed by quantifying the extravasation of EB in the heart at 24 h after LPS treatment. Frozen heart sections (G) were observed under a confocal LSM 710 microscope. Blue represents DAPI, and red represents EB; scale bars, 50 μm. The relative intensity of red fluorescence emitted by EB was quantified (H) with ImageJ software (n = 4–5). (I) Mouse cardiac endothelial cells (MCECs) (on the insert of transwell) were cultured in the presence or absence of RPMs on the bottom chamber for 4 days until the endothelial monolayer was established. Then fluorescein isothiocyanate (FITC)-dextran particle was added into the upper insert, and thrombin (3 U/mL) was used to stimulate MCECs for 1 h. The degree of EC monolayer leakage was determined by measuring the intensity of FITC-dextran fluorescence in the basolateral chamber (n = 4). (J–L) MCECs were cultured in the control medium (C-M) or RPM conditioned medium (RPM-M) for 1 day. qRT-PCR was used to determine mRNA levels of ZO-1 (J), VE-cadherin (K), and occludin (L), in the presence or absence of RPM conditioned medium (n = 4). (M) MCECs were cultured with control medium or RPM conditioned medium for 3 days to reach the monolayer on the coverslip. Representative images of immunofluorescent staining for ZO-1 (green) at 1 h after thrombin (3 U/mL) or PMA (40 ng/mL) treatment. White arrows indicate the integrity linear pattern of ZO-1. Yellow arrows present the fragmentations and depletions of ZO-1. Scale bars, 20 μm. All results are presented as mean ± SEM and analyzed by Student's t test or one-way ANOVA.

DISCUSSION

In this study, we demonstrated that LPS administration dramatically reduced the TRM population along with the recruitment of inflammatory monocytes and neutrophils in multiple organs. Notably, Sectm1a null mice had a smaller TRM population and more inflammatory monocytes and neutrophils in organs, which were associated with more than severe organ damage compared with WT mice upon LPS insult. Both our *in vitro* and *in vivo* data showed that Sectm1a was able to promote TRM proliferation through boosting Th cells and driving the release of cytokines (i.e., IL-4, GM-CSF, and M-CSF).

Importantly, we identified that GITR, as a receptor of Sectm1a, was essential for Th cell-mediated boosting effects on macrophage self-renewal. Furthermore, we found that TRMs played a critical role in maintaining local vascular integrity. Collectively, our study uncovers that Sectm1a could positively regulate local proliferation of TRMs in the context of acute inflammation.

Recently, TRMs have been shown to play important roles in maintaining organ homeostasis, maintaining immune defense, and promoting tissue healing during inflammatory diseases, and maintaining an appropriate size of TRM pool has the potential to preserve and restore tissue homeostasis upon acute inflammation challenge.[46] In line with our study, Shults et al.[47] reported that AMs were diminished by 50% in the bronchoalveolar lavage (BAL) at 24 h after burn injury and binge ethanol intoxication. In addition, the reduction of CRM was also observed in numerous mouse models of cardiac disease, including permanent myocardial infarction, reperfused myocardial infarction, and diphtheria toxin cardiomyocyte ablation.[48,49] These reductions have mainly been attributed to increased cell death.[50] However, the self-renewal capacity, as the most important trait of TRMs, has been overlooked, and it remains unclear how to modulate the self-renewal capacity of TRMs in inflammatory diseases.[46] In the present study, using a global KO mouse model, we observed that loss of Sectm1a impaired self-renewal capacity of residential macrophages in the spleen, lung, and heart of mice during acute inflammation. By contrast, administration of mice with rSectm1a protein attenuated LPS-induced reduction of TRMs and, in turn, improved mouse survival.

Our mechanistic study reveals that rSectm1a-mediated beneficial effects rely on the crosstalk between Th cells and macrophages in a GITR-dependent manner. GITR serves as a receptor of Sectm1a on T cells,[23] and such interaction of Sectm1a/GITR could promote the expansion of Th cells and the release of cytokine, leading to positive regulation on the proliferation of TRMs. Although GITR was previously thought to be a marker of Treg (regulatery T cell) precursor cells, recent studies have demonstrated that GITR is highly expressed in the activated $CD4^+$ T cells.[51–54] Functionally, in addition to stimulating the proliferation and differentiation of $CD4^+$ naive T cells, GITR is also engaged in promoting the cytokine release from fully polarized Th2,[55–57] leading to a positive feedback on Th2 differentiation and cytokine production. Consistent with these reports, using co-culture of naive CD4 T cells with macrophages, we observed that rSectm1a treatment increased the Th2 population to a greater degree than the Th1 population regardless of LPS stimulation, indicating a skewing effect on Th2 polarization. Furthermore, it was reported that the activation of GITR increased T cell survival and abrogated the suppressive action of Treg cells.[58,59] Regarding the factors/signals that stimulate self-renewal of TRMs, several cytokines (i.e., IL-4, GM-CSF, M-CSF, and IL-34) have been validated thus far.[9,60] Nonetheless, among these stimulators, GM-CSF, M-CSF, and IL-34 are all context and tissue specific in promoting TRM proliferation,[9] and only IL-4 is able to induce rapid local proliferation in diverse tissues.[44,45,61] Therefore, our present work, together with these prior studies, supports that Sectm1a, as a novel GITR ligand, promotes the expansion of Th cells, especially Th2, and increases secretion of Th2 cytokines, which, in turn, stimulate the local proliferation of TRMs and improve animal survival following endotoxin treatment. Consistent with our findings, Scumpia et al.[62] observed that treatment of mice with DTA-1, a GITR ligand, restored $CD4^+$ T cell proliferation, increased Th2 cytokine production, and improved survival in mice after injection of bacteria. In addition, after analyzing >150 million human patients in the Truven MarketScan insurance claim database, Krishack et al.[63] found that patients with activation of type 2 allergic immune response (characterized by the expansion of Th2 and production of Th2 cytokines) possess a significantly lower incidence of sepsis and/or sepsis-related mortality, suggesting that pre-existing Th2 activation could protect against the development of sepsis.

Although TRMs are known to promote angiogenesis in the context of tumor growth,[64] whether TRMs influence vascular integrity during sepsis remains unclear. Under sepsis condition, loss of endothelial barrier accounts for the vascular leakage and contributes to infiltration of leukocytes, tissue edema, and organ damage.[65,66] In the present study, using *in vitro* splenic RPMs as a model of TRMs, we observed that RPMs helped to maintain EC monolayer integrity by upregulation of tight-junction-associated proteins (i.e., ZO-1, Occludin, and VE-Cadherin). Furthermore, pre-depletion of TRM *in vivo* augmented LPS-induced vascular leakage in multiple organs of mice. Together, both *in vitro* and *in vivo* data suggest that TRMs (especially those located near vessels) may work as a "gatekeeper" and play a pivotal role in maintaining the vascular integrity. Therefore, the elevation of TRMs may protect against sepsis-induced vascular hyper-permeability and organ failure.

Currently, it is well recognized that there is a special monocyte reservoir in the spleen (splenic reservoir monocytes). As a major source of monocytes, splenic monocytes egress from the spleen, migrate to sites of inflammation, and promote chronic inflammation and organ damages in response to myocardial infarct, stroke, and atherosclerosis.[34–37] Nevertheless, how to regulate such monocyte migration from spleen to other organs remains obscure. In the present study, we observed that global depletion of Sectm1a in mice caused more release of splenic monocytes, contributing to the further infiltration of inflammatory monocytes into the lung and the heart compared with WT mice following endotoxin treatment. By contrast, administration of mice with rSectm1a protein exhibited the opposite effects. These findings suggest that Sectm1a may be a critical factor to coordinate crosstalk between spleen and other organs during sepsis.

Some limitations of our study should be acknowledged. Although our data show that TRMs are essential for maintaining local vascular integrity during acute inflammation, the further molecular mechanism behind this needs to be explored in the future. In addition to causing pulmonary failure and cardiovascular dysfunction, severe sepsis also resulted in other organ dysfunctions, such as kidney dysfunction (reduced urine volume) and liver dysfunction (jaundice and cholestasis). Thus, in the future, the population change of TRM

at the earlier stage of acute inflammation should also be determined in other organs. Furthermore, although the data in this study focused on Sectm1a's effects during early inflammatory insults, we did not investigate its effects at a later stage, the inflammation resolution phase. During this phase, TRMs would undergo a transient and intense proliferative burst *in situ* to repopulate the tissue and facilitate tissue repair processes.[46] Interestingly, our results showed that the gene expression levels of Sectm1a in the lung and heart were significantly increased at a later time point after LPS treatment, implying a positive regulatory effect of Sectm1a on the self-renewal capacity of TRMs during the inflammation resolution phase. Besides, given that the successive loss in self-renewal capacity with age may help to explain the dramatic increases of sepsis incidence and mortality rates among aged patients ($\geq$65 years) compared with younger patients,[17–19,46] it would be very interesting and important to decipher the role of Sectm1a in mediating the local proliferation of TRM in aged mice, which might have a great biomedical potential. Together, future new discoveries in the field of TRMs would be very helpful in the development of novel drugs that treat a wide range of acute inflammatory diseases.

MATERIALS AND METHODS

Mice

All mice were maintained and bred under specific pathogen-free conditions in the Division of Laboratory Animal Resources at the University of Cincinnati Medical Center. All animal experiments conformed to the Guidelines for the Care and Use of Laboratory Animals prepared by the National Academy of Sciences, published by the National Institutes of Health, and approved by the University of Cincinnati Animal Care and Use Committee. The mouse models used in this study were described in the electronic supplementary material.

Cell Culture

We isolated naïve $CD4^+$ T cells and $CD4^+$ T cell from mouse spleen by using EasySep Mouse Naïve $CD4^+$ T Cell Isolation Kit (STEMCELL) and EasySep™ Mouse $CD4^+$ T Cell Isolation Kit (STEMCELL), respectively. The detailed cell preparations and cell culture conditions of $CD4^+$ T Cell, RPMs, and mouse cardiac endothelial cells (MCECs) were briefly described in the electronic supplementary material.

Flow Cytometry Analysis

Single-cell suspensions were prepared according to previous studies, which are described in the Supplemental Materials and Methods. Cells were stained with LIVE/DEAD Fixable Blue Dead Cell Stain Kit (Invitrogen) for the detection of live/dead cells before staining of the cell surface. A CD16/32 antibody (clone 93) (eBioscience, 1:100 dilution) was used to block the non-specific binding to Fc receptors before surface staining. All antibodies used in this study are listed in Table S3. The detailed method descriptions for the surface marker staining and intracellular Ki-67 staining are available in the Supplemental Materials and Methods.

Co-culture of RPMs with Naïve CD4 T Cells

RPMs were seeded on the coverslip at the same density (1×10^5) and cultured on the lower chamber of Transwell (Corning Life Sciences). Before co-culture, the insert was coated with IgG2a (1.25 μg/mL) or rSectm1a (2 μg/mL) at 4°C for 24 h. Naïve $CD4^+$ T cells were isolated from spleen by using EasySep Mouse Naïve $CD4^+$ T Cell Isolation Kit (STEMCELL) and cultured on the pre-coated insert (1.5×10^6/insert). At the same time, Dynabeads covalently coupled to anti-CD3, and anti-CD28 antibodies were added to stimulate naïve CD4 T cells. After 4 days stimulation, half of the Transwells were treated with 200 ng/mL LPS for 2 days. Then, supernatants were collected to determine the cytokine level. RPMs were stained with EdU (green) and F4/80 (red). Meanwhile, intracellular cytokine assays for IFN-γ and IL-4 were carried out following PMA (20 ng/mL) and ionomycin (1 μg/mL) stimulation to determine the Th1 and Th2 differentiation.

EdU Incorporation Assay and Immunofluorescence Stain

EdU (Click-iT EdU Cell Proliferation Imaging Kit, Invitrogen) is a nucleoside analog of thymidine. It is incorporated into DNA during active DNA synthesis. Cell proliferation was determined by the EdU incorporation assay according to the manufacturer's instruction. After co-culture, RPMs were incubated with an EdU-labeling solution for 6 h at 37°C and then fixed with 4% cold formaldehyde for 30 min at room temperature. After permeabilization with 1% Triton X-100, cells were reacted with Click-iT reaction cocktails (Invitrogen) for 30 min. After washing, cells were incubated with PE-conjugated anti-mouse F4/80 for 1 h at room temperature. Subsequently, the DNA contents of the cells were stained with Hoechst 33342 for 30 min. Finally, cells were mounted with ProLong Diamond Antifade Mounting medium with DAPI (Invitrogen). Images were captured with Zeiss LSM710 LIVE Duo Confocal Microscope (Live Microscopy Core, University of Cincinnati). The detailed immunofluorescence stain method descriptions are available in the Supplemental Materials and Methods.

Measurement of Vascular Leakage in Multiple Organs

The pulmonary microvascular permeability was determined in each experimental group by measuring the EB accumulation in lung tissue and lung wet to dry weight ratio. The detailed methods are described in the Supplemental Materials and Methods. For the measurement of cardiac vascular permeability, EB accumulation in the heart was determined as described previously, which is also briefly described in the Supplemental Materials and Methods.

Spleen/Lung Histology and Injury Score

The spleen and lung tissues were collected from mice at 24 h post-LPS injection. The detailed histology and injury score method descriptions are available in the Supplemental Materials and Methods.

In Vitro Endothelial Permeability Assay

MCECs (8×10^4 cells/well) were seeded on the insert of 12-well Transwell (Corning) and cultured in the presence or absence of RPMs for 3 days to form a monolayer. Just before stimulating ECs with thrombin (Sigma) (5 U/mL), the fluorescein isothiocyanate (FITC)-dextran (10 kDa) (Sigma) stock solution was added to the medium on the insert to achieve a final concentration of 1 mg/mL. After

30 min, 50 μL samples of the medium were taken in triplicate from the lower chamber and placed in a 96-well cluster plate to measure the fluorescent intensity (excitation at 485 nm and emission at 535 nm).

RNA Isolation and Quantitative RT-PCR (qRT-PCR)

Total RNA was extracted from cultured cells or tissues by using the RNeasy Kit (Qiagen) following the manufacturer's manual. cDNA was synthesized from 0.5–1.0 μg RNA by using Superscript II Reverse Transcriptase (Invitrogen). Then, qRT-PCR was performed in triplicate with the ABI PRISM 7900HT Sequence Detection System (ABI) using SYBR green (Genecopoeia). Relative mRNA levels were calculated and normalized to 18S rRNA. The primers were as follows: ZO-1 forward 5′-GCTAAGAGCACAGCAATGGA-3′, reverse 5′GC ATGTTCAACGTTATCCAT; VE-cadherin forward 5′-TCTTGCC AGCAAACTCTCCT-3′, reverse 5′-TTGGAATCAAATGCACAT CG-3′; Occludin forward 5′-GGACCCTGACCACTATGAAACAGA CTAC-3′, reverse 5′-ATAGGTGGATATTCCCTGACCCAGTC-3′; Sectm1a forward 5′-ATGATGACCTGCCCTTCAGTGC-3′, reverse 5′-CTGGGTGTCTTTGATCACAAGC-3′; and 18S rRNA forward 5′-GCAATTATTCCCCATGAACG-3′, reverse 5′-GGCCTCACTAA ACCATCCAA-3′.

Measurement of Cytokines

Blood was collected 12 h after LPS injection, and plasma samples were prepared by centrifugation at 3000 × g for 15 min at 4°C. Cell culture supernatants from RPM and naïve CD4 T cell co-culture experiments were collected and centrifugation at 800 × g for 15 min at 4°C to remove cell debris. All plasmas and cell culture supernatants were put into -80 °C until use. The concentration of cytokines was measured using Luminex Multiplex Immunoassay (Invitrogen) according to the manufacturer's protocol.

Western Blot Analysis

The total protein was extracted from MCECs cultured with control medium or RPM-conditioned medium. Equal amounts of protein were subjected to SDS-PAGE and gel electrophoresis as described in a previous study.[1] The following antibodies were used: rabbit anti-ZO-1 (61-7300) (1:250; ThermoFisher); rabbit anti-VE-Cadherin (ab33168) (1:500; Abcam); and rabbit anti-GAPDH (1:1000; Cell Signaling Technology).

Statistical Analysis

All data were tested for normality with Shapiro-Wilks test before statistical analysis. Statistical calculations were performed with GraphPad Prism 5.0 and all data were presented as mean ± SEM. Data were analyzed using two tailed Student's t test (normally distributed data) or Mann-Whitney test (non-normally distributed data) to determine the significance between population means when two groups were compared. For comparison of more than two groups, one-way ANOVA or two-way ANOVA were used to determine the significance. The survival rates were constructed using the Kaplan-Meier method, and differences in mortality were compared using log-rank (Mantel-Cox) test. A $p < 0.05$ was considered statistically significant.

SUPPLEMENTAL INFORMATION

Supplemental Information can be found online at https://doi.org/10.1016/j.ymthe.2020.12.001.

ACKNOWLEDGMENTS

This study was partially supported by the National Institutes of Health (NIH) (grants R01 GM-126061 and GM-132149) and American Heart Association (AHA) Established Investigator Award (17EIA33400063 to G.-C.F.).

AUTHOR CONTRIBUTIONS

X.M. conceived the project, designed and performed experiments, and wrote the manuscript. H.F. measured the plasma level of Sectm1 in sepsis patients and healthy donors. P.W., K.E., Y.L., and Q.L. helped to sacrifice mice and collect samples. P.W. and K.D. helped to conduct flow cytometry experiments. Y.L. and X.W. reviewed/edited the manuscript. J.C. and T.P helped to analyze data. G.-C.F. analyzed results, reviewed/edited the manuscript, provided financial and administrative support, and gave final approval of the manuscript.

DECLARATION OF INTEREST

The authors declare no competing interests.

REFERENCES

1. Fleischmann, C., Scherag, A., Adhikari, N.K., Hartog, C.S., Tsaganos, T., Schlattmann, P., Angus, D.C., and Reinhart, K.; International Forum of Acute Care Trialists (2016). Assessment of Global Incidence and Mortality of Hospital-treated Sepsis. Current Estimates and Limitations. Am. J. Respir. Crit. Care Med. *193*, 259–272.

2. Paoli, C.J., Reynolds, M.A., Sinha, M., Gitlin, M., and Crouser, E. (2018). Epidemiology and Costs of Sepsis in the United States-An Analysis Based on Timing of Diagnosis and Severity Level. Crit. Care Med. *46*, 1889–1897.

3. Gaieski, D.F., Edwards, J.M., Kallan, M.J., and Carr, B.G. (2013). Benchmarking the incidence and mortality of severe sepsis in the United States. Crit. Care Med. *41*, 1167–1174.

4. Hershey, T.B., and Kahn, J.M. (2017). State Sepsis Mandates – A New Era for Regulation of Hospital Quality. N. Engl. J. Med. *376*, 2311–2313.

5. Dunn, D.L. (2000). Prevention and treatment of multiple organ dysfunction syndrome: lessons learned and future prospects. Surg. Infect. (Larchmt.) *1*, 227–236, discussion 236–237.

6. Opal, S.M. (2010). Endotoxins and other sepsis triggers. In Endotoxemia and Endotoxin Shock, C. Ronco, ed. (Karger Publishers), pp. 14–24.

7. Hotchkiss, R.S., Moldawer, L.L., Opal, S.M., Reinhart, K., Turnbull, I.R., and Vincent, J.L. (2016). Sepsis and septic shock. Nat. Rev. Dis. Primers *2*, 16045.

8. Kumar, V. (2018). Targeting macrophage immunometabolism: Dawn in the darkness of sepsis. Int. Immunopharmacol. *58*, 173–185.

9. Sieweke, M.H., and Allen, J.E. (2013). Beyond stem cells: self-renewal of differentiated macrophages. Science *342*, 1242974.

10. Hashimoto, D., Chow, A., Noizat, C., Teo, P., Beasley, M.B., Leboeuf, M., Becker, C.D., See, P., Price, J., Lucas, D., et al. (2013). Tissue-resident macrophages self-maintain locally throughout adult life with minimal contribution from circulating monocytes. Immunity *38*, 792–804.

11. Sheng, J., Ruedl, C., and Karjalainen, K. (2015). Most tissue-resident macrophages except microglia are derived from fetal hematopoietic stem cells. Immunity *43*, 382–393.

12. Ginhoux, F., and Guilliams, M. (2016). Tissue-resident macrophage ontogeny and homeostasis. Immunity *44*, 439–449.

13. Epelman, S., Lavine, K.J., and Randolph, G.J. (2014). Origin and functions of tissue macrophages. Immunity *41*, 21–35.

14. Shi, C., and Pamer, E.G. (2011). Monocyte recruitment during infection and inflammation. Nat. Rev. Immunol. *11*, 762–774.

15. Roberts, A.W., Lee, B.L., Deguine, J., John, S., Shlomchik, M.J., and Barton, G.M. (2017). Tissue-resident macrophages are locally programmed for silent clearance of apoptotic cells. Immunity *47*, 913–927.e6.

16. Uderhardt, S., Martins, A.J., Tsang, J.S., Lämmermann, T., and Germain, R.N. (2019). Resident macrophages cloak tissue microlesions to prevent neutrophil-driven inflammatory damage. Cell *177*, 541–555.e17.

17. Molawi, K., Wolf, Y., Kandalla, P.K., Favret, J., Hagemeyer, N., Frenzel, K., Pinto, A.R., Klapproth, K., Henri, S., Malissen, B., et al. (2014). Progressive replacement of embryo-derived cardiac macrophages with age. J. Exp. Med. *211*, 2151–2158.

18. Gentek, R., Molawi, K., and Sieweke, M.H. (2014). Tissue macrophage identity and self-renewal. Immunol. Rev. *262*, 56–73.

19. Hoeffel, G., and Ginhoux, F. (2015). Ontogeny of tissue-resident macrophages. Front. Immunol. *6*, 486.

20. Chmielewski, S., Olejnik, A., Sikorski, K., Pelisek, J., Błaszczyk, K., Aoqui, C., Nowicka, H., Zernecke, A., Heemann, U., Wesoly, J., et al. (2014). STAT1-dependent signal integration between IFNγ and TLR4 in vascular cells reflect pro-atherogenic responses in human atherosclerosis. PLoS ONE *9*, e113318.

21. Li, Y., Lua, I., French, S.W., and Asahina, K. (2016). Role of TGF-β signaling in differentiation of mesothelial cells to vitamin A-poor hepatic stellate cells in liver fibrosis. Am. J. Physiol. Gastrointest. Liver Physiol. *310*, G262–G272.

22. Kamata, H., Yamamoto, K., Wasserman, G.A., Zabinski, M.C., Yuen, C.K., Lung, W.Y., Gower, A.C., Belkina, A.C., Ramirez, M.I., Deng, J.C., et al. (2016). Epithelial cell–derived secreted and transmembrane 1a signals to activated neutrophils during pneumococcal pneumonia. Am. J. Respir. Cell Mol. Biol. *55*, 407–418.

23. Howie, D., Garcia Rueda, H., Brown, M.H., and Waldmann, H. (2013). Secreted and transmembrane 1A is a novel co-stimulatory ligand. PLoS ONE *8*, e73610.

24. Lyman, S.D., Escobar, S., Rousseau, A.M., Armstrong, A., and Fanslow, W.C. (2000). Identification of CD7 as a cognate of the human K12 (SECTM1) protein. J. Biol. Chem. *275*, 3431–3437.

25. Wang, T., Huang, C., Lopez-Coral, A., Slentz-Kesler, K.A., Xiao, M., Wherry, E.J., and Kaufman, R.E. (2012). K12/SECTM1, an interferon-γ regulated molecule, synergizes with CD28 to costimulate human T cell proliferation. J. Leukoc. Biol. *91*, 449–459.

26. Tsalik, E.L., Langley, R.J., Dinwiddie, D.L., Miller, N.A., Yoo, B., van Velkinburgh, J.C., Smith, L.D., Thiffault, I., Jaehne, A.K., Valente, A.M., et al. (2014). An integrated transcriptome and expressed variant analysis of sepsis survival and death. Genome Med. *6*, 111.

27. Bronte, V., and Pittet, M.J. (2013). The spleen in local and systemic regulation of immunity. Immunity *39*, 806–818.

28. Edgren, G., Almqvist, R., Hartman, M., and Utter, G.H. (2014). Splenectomy and the risk of sepsis: a population-based cohort study. Ann. Surg. *260*, 1081–1087.

29. Liu, Y.C., Yu, M.M., Shou, S.T., and Chai, Y.F. (2017). Sepsis-induced cardiomyopathy: mechanisms and treatments. Front. Immunol. *8*, 1021.

30. Mu, X., Wang, X., Huang, W., Wang, R.T., Essandoh, K., Li, Y., Pugh, A.M., Peng, J., Deng, S., Wang, Y., et al. (2018). Circulating Exosomes Isolated from Septic Mice Induce Cardiovascular Hyperpermeability Through Promoting Podosome Cluster Formation. Shock *49*, 429–441.

31. Yona, S., Kim, K.W., Wolf, Y., Mildner, A., Varol, D., Breker, M., Strauss-Ayali, D., Viukov, S., Guilliams, M., Misharin, A., et al. (2013). Fate mapping reveals origins and dynamics of monocytes and tissue macrophages under homeostasis. Immunity *38*, 79–91.

32. Davies, L.C., Jenkins, S.J., Allen, J.E., and Taylor, P.R. (2013). Tissue-resident macrophages. Nat. Immunol. *14*, 986–995.

33. Borges da Silva, H., Fonseca, R., Pereira, R.M., Cassado, Ados.A., Álvarez, J.M., and D'Império Lima, M.R. (2015). Splenic macrophage subsets and their function during blood-borne infections. Front. Immunol. *6*, 480.

34. Swirski, F.K., Nahrendorf, M., Etzrodt, M., Wildgruber, M., Cortez-Retamozo, V., Panizzi, P., Figueiredo, J.L., Kohler, R.H., Chudnovskiy, A., Waterman, P., et al. (2009). Identification of splenic reservoir monocytes and their deployment to inflammatory sites. Science *325*, 612–616.

35. Francis, M., Sun, R., Cervelli, J.A., Choi, H., Mandal, M., Abramova, E.V., Gow, A.J., Laskin, J.D., and Laskin, D.L. (2017). Editor's highlight: Role of spleen-derived macrophages in ozone-induced lung inflammation and injury. Toxicol. Sci. *155*, 182–195.

36. Leuschner, F., Panizzi, P., Chico-Calero, I., Lee, W.W., Ueno, T., Cortez-Retamozo, V., Waterman, P., Gorbatov, R., Marinelli, B., Iwamoto, Y., et al. (2010). Angiotensin-converting enzyme inhibition prevents the release of monocytes from their splenic reservoir in mice with myocardial infarction. Circ. Res. *107*, 1364–1373.

37. Hsiao, H.M., Fernandez, R., Tanaka, S., Li, W., Spahn, J.H., Chiu, S., Akbarpour, M., Ruiz-Perez, D., Wu, Q., Turam, C., et al. (2018). Spleen-derived classical monocytes mediate lung ischemia-reperfusion injury through IL-1β. J. Clin. Invest. *128*, 2833–2847.

38. Rose, S., Misharin, A., and Perlman, H. (2012). A novel Ly6C/Ly6G-based strategy to analyze the mouse splenic myeloid compartment. Cytometry A *81*, 343–350.

39. Hussell, T., and Bell, T.J. (2014). Alveolar macrophages: plasticity in a tissue-specific context. Nat. Rev. Immunol. *14*, 81–93.

40. Frantz, S., and Nahrendorf, M. (2014). Cardiac macrophages and their role in ischaemic heart disease. Cardiovasc. Res. *102*, 240–248.

41. Aurora, A.B., Porrello, E.R., Tan, W., Mahmoud, A.I., Hill, J.A., Bassel-Duby, R., Sadek, H.A., and Olson, E.N. (2014). Macrophages are required for neonatal heart regeneration. J. Clin. Invest. *124*, 1382–1392.

42. Hulsmans, M., Clauss, S., Xiao, L., Aguirre, A.D., King, K.R., Hanley, A., Hucker, W.J., Wülfers, E.M., Seemann, G., Courties, G., et al. (2017). Macrophages facilitate electrical conduction in the heart. Cell *169*, 510–522.e20.

43. Mu, X., Wang, P., Wang, X., Li, Y., Zhao, H., Li, Q., Essandoh, K., Deng, S., Peng, T., and Fan, G.C. (2020). Identification of a Novel Antisepsis Pathway: Sectm1a Enhances Macrophage Phagocytosis of Bacteria through Activating GITR. J. Immunol. *205*, 1633–1643.

44. Jenkins, S.J., Ruckerl, D., Cook, P.C., Jones, L.H., Finkelman, F.D., van Rooijen, N., MacDonald, A.S., and Allen, J.E. (2011). Local macrophage proliferation, rather than recruitment from the blood, is a signature of TH2 inflammation. Science *332*, 1284–1288.

45. Jenkins, S.J., Ruckerl, D., Thomas, G.D., Hewitson, J.P., Duncan, S., Brombacher, F., Maizels, R.M., Hume, D.A., and Allen, J.E. (2013). IL-4 directly signals tissue-resident macrophages to proliferate beyond homeostatic levels controlled by CSF-1. J. Exp. Med. *210*, 2477–2491.

46. Mu, X., Li, Y., and Fan, G.C. (2021). Tissue-Resident Macrophages in the Control of Infection and Resolution of Inflammation. Shock *55*, 14–23.

47. Shults, J.A., Curtis, B.J., Boe, D.M., Ramirez, L., and Kovacs, E.J. (2016). Ethanol intoxication prolongs post-burn pulmonary inflammation: role of alveolar macrophages. J. Leukoc. Biol. *100*, 1037–1045.

48. Bajpai, G., Bredemeyer, A., Li, W., Zaitsev, K., Koenig, A.L., Lokshina, I., Mohan, J., Ivey, B., Hsiao, H.M., Weinheimer, C., et al. (2019). Tissue resident CCR2^{-} and CCR2^{+} cardiac macrophages differentially orchestrate monocyte recruitment and fate specification following myocardial injury. Circ. Res. *124*, 263–278.

49. Honold, L., and Nahrendorf, M. (2018). Resident and monocyte-derived macrophages in cardiovascular disease. Circ. Res. *122*, 113–127.

50. Barth, M.W., Hendrzak, J.A., Melnicoff, M.J., and Morahan, P.S. (1995). Review of the macrophage disappearance reaction. J. Leukoc. Biol. *57*, 361–367.

51. Kanamaru, F., Youngnak, P., Hashiguchi, M., Nishioka, T., Takahashi, T., Sakaguchi, S., Ishikawa, I., and Azuma, M. (2004). Costimulation via glucocorticoid-induced TNF receptor in both conventional and CD25^{+} regulatory CD4^{+} T cells. J. Immunol. *172*, 7306–7314.

52. Nocentini, G., Giunchi, L., Ronchetti, S., Krausz, L.T., Bartoli, A., Moraca, R., Migliorati, G., and Riccardi, C. (1997). A new member of the tumor necrosis factor/nerve growth factor receptor family inhibits T cell receptor-induced apoptosis. Proc. Natl. Acad. Sci. USA *94*, 6216–6221.

53. Kwon, B., Yu, K.Y., Ni, J., Yu, G.L., Jang, I.K., Kim, Y.J., Xing, L., Liu, D., Wang, S.X., and Kwon, B.S. (1999). Identification of a novel activation-inducible protein of the tumor necrosis factor receptor superfamily and its ligand. J. Biol. Chem. *274*, 6056–6061.

54. Clouthier, D.L., and Watts, T.H. (2014). Cell-specific and context-dependent effects of GITR in cancer, autoimmunity, and infection. Cytokine Growth Factor Rev. *25*, 91–106.

55. Motta, A.C., Vissers, J.L., Gras, R., Van Esch, B.C., Van Oosterhout, A.J., and Nawijn, M.C. (2009). GITR signaling potentiates airway hyperresponsiveness by enhancing Th2 cell activity in a mouse model of asthma. Respir. Res. *10*, 93.

56. van der Werf, N., Redpath, S.A., Phythian-Adams, A.T., Azuma, M., Allen, J.E., Maizels, R.M., Macdonald, A.S., and Taylor, M.D. (2011). Th2 responses to helminth parasites can be therapeutically enhanced by, but are not dependent upon, GITR-GITR ligand costimulation in vivo. J. Immunol. *187*, 1411–1420.

57. Ward-Kavanagh, L.K., Lin, W.W., Šedý, J.R., and Ware, C.F. (2016). The TNF receptor superfamily in co-stimulating and co-inhibitory responses. Immunity *44*, 1005–1019.

58. Shevach, E.M., and Stephens, G.L. (2006). The GITR-GITRL interaction: co-stimulation or contrasuppression of regulatory activity? Nat. Rev. Immunol. *6*, 613–618.

59. Esparza, E.M., and Arch, R.H. (2005). Glucocorticoid-induced TNF receptor functions as a costimulatory receptor that promotes survival in early phases of T cell activation. J. Immunol. *174*, 7869–7874.

60. Röszer, T. (2018). Understanding the biology of self-renewing macrophages. Cells *7*, 103.

61. Minutti, C.M., Jackson-Jones, L.H., García-Fojeda, B., Knipper, J.A., Sutherland, T.E., Logan, N., Ringqvist, E., Guillamat-Prats, R., Ferenbach, D.A., Artigas, A., et al. (2017). Local amplifiers of IL-4Rα-mediated macrophage activation promote repair in lung and liver. Science *356*, 1076–1080.

62. Scumpia, P.O., Delano, M.J., Kelly-Scumpia, K.M., Weinstein, J.S., Wynn, J.L., Winfield, R.D., Xia, C., Chung, C.S., Ayala, A., Atkinson, M.A., et al. (2007). Treatment with GITR agonistic antibody corrects adaptive immune dysfunction in sepsis. Blood *110*, 3673–3681.

63. Krishack, P.A., Wang, K., Rzhetsky, A., Solway, J., Sperling, A.I., and Verhoef, P.A. (2017). Preexisting type 2 immune activation protects against the development of sepsis. Am. J. Respir. Cell Mol. Biol. *57*, 628–630.

64. Poh, A.R., and Ernst, M. (2018). Targeting macrophages in cancer: from bench to bedside. Front. Oncol. *8*, 49.

65. Kadl, A., and Leitinger, N. (2005). The role of endothelial cells in the resolution of acute inflammation. Antioxid. Redox Signal. *7*, 1744–1754.

66. Leenders, G.J., Smeets, M.B., van den Boomen, M., Berben, M., Nabben, M., van Strijp, D., Strijkers, G.J., Prompers, J.J., Arslan, F., Nicolay, K., and Vandoorne, K. (2018). Statins promote cardiac infarct healing by modulating endothelial barrier function revealed by contrast-enhanced magnetic resonance imaging. Arterioscler. Thromb. Vasc. Biol. *38*, 186–194.

YMTHE, Volume *29*

Supplemental Information

Sectm1a Facilitates Protection against Inflammation-Induced Organ Damage through Promoting TRM Self-Renewal

Xingjiang Mu, Hongkuan Fan, Peng Wang, Yutian Li, Karen Domenico, Qianqian Li, Xiaohong Wang, Kobina Essandoh, Jing Chen, Tianqing Peng, and Guo-Chang Fan

Supplemental figures

Figure S1

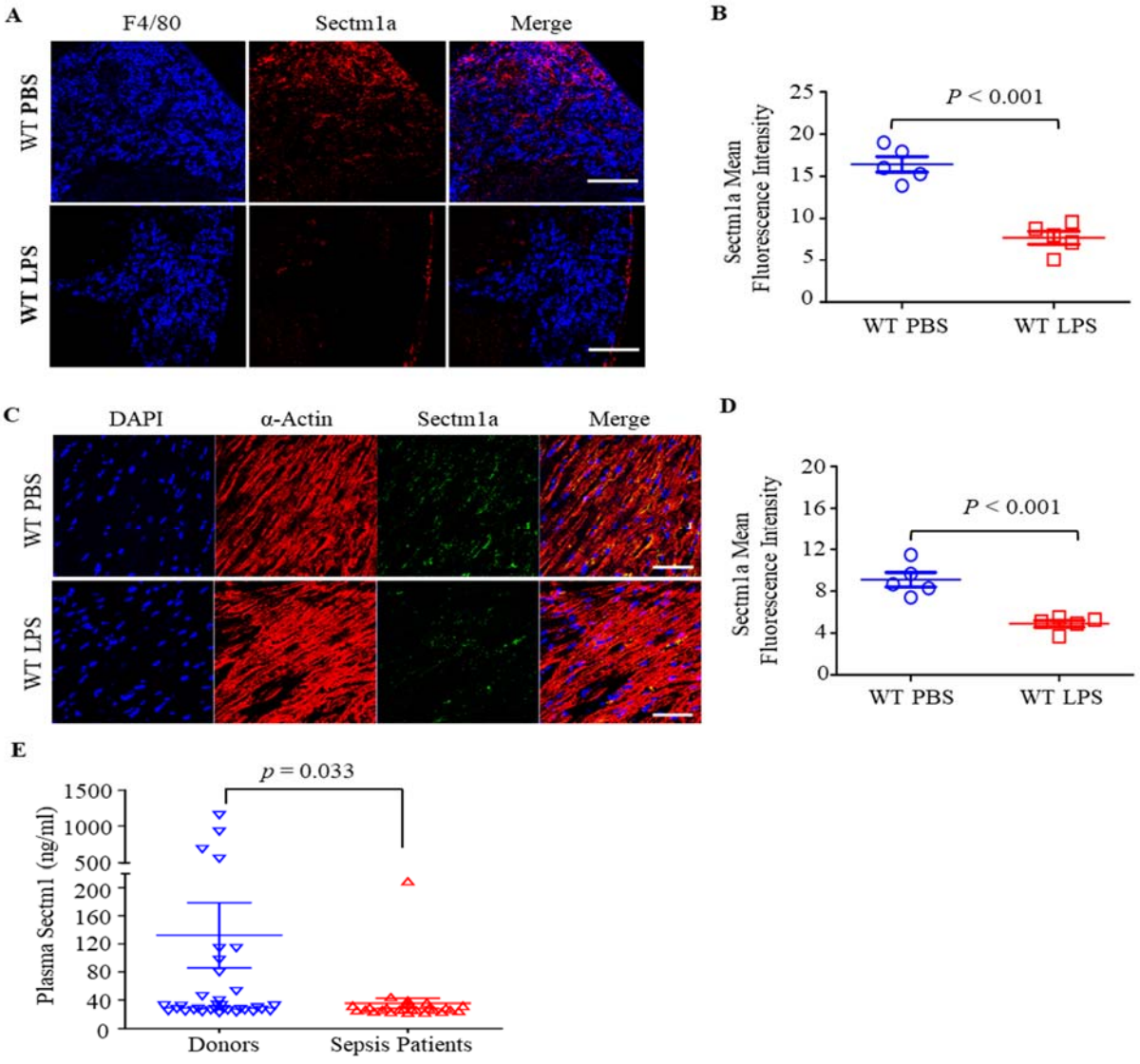

Figure S1. The spleen and heart tissues in WT mice were collected at 18 h after PBS or LPS injection and subjected to immunofluorescent staining. (A) Representative immunofluorescence staining image for Sectm1a in the spleen. Sectm1a (Red), F4/80 (Blue). Scale bar: 100 μm (B) The mean of red fluorescence intensity in view field was quantified with Image J. n = 5. (C) Representative immunofluorescence staining image for Sectm1a (Green) in the heart. α-Actin (Red), Sectm1a (Green), DAPI (Blue). Scale bar: 50 μm (D) The mean of green fluorescence intensity in view field of heart was quantified with Image J. n = 5. (E) Plasma SECTM1 levels were quantified by ELISA in septic patients (n = 27) and healthy donors (n = 34).

Figure S2

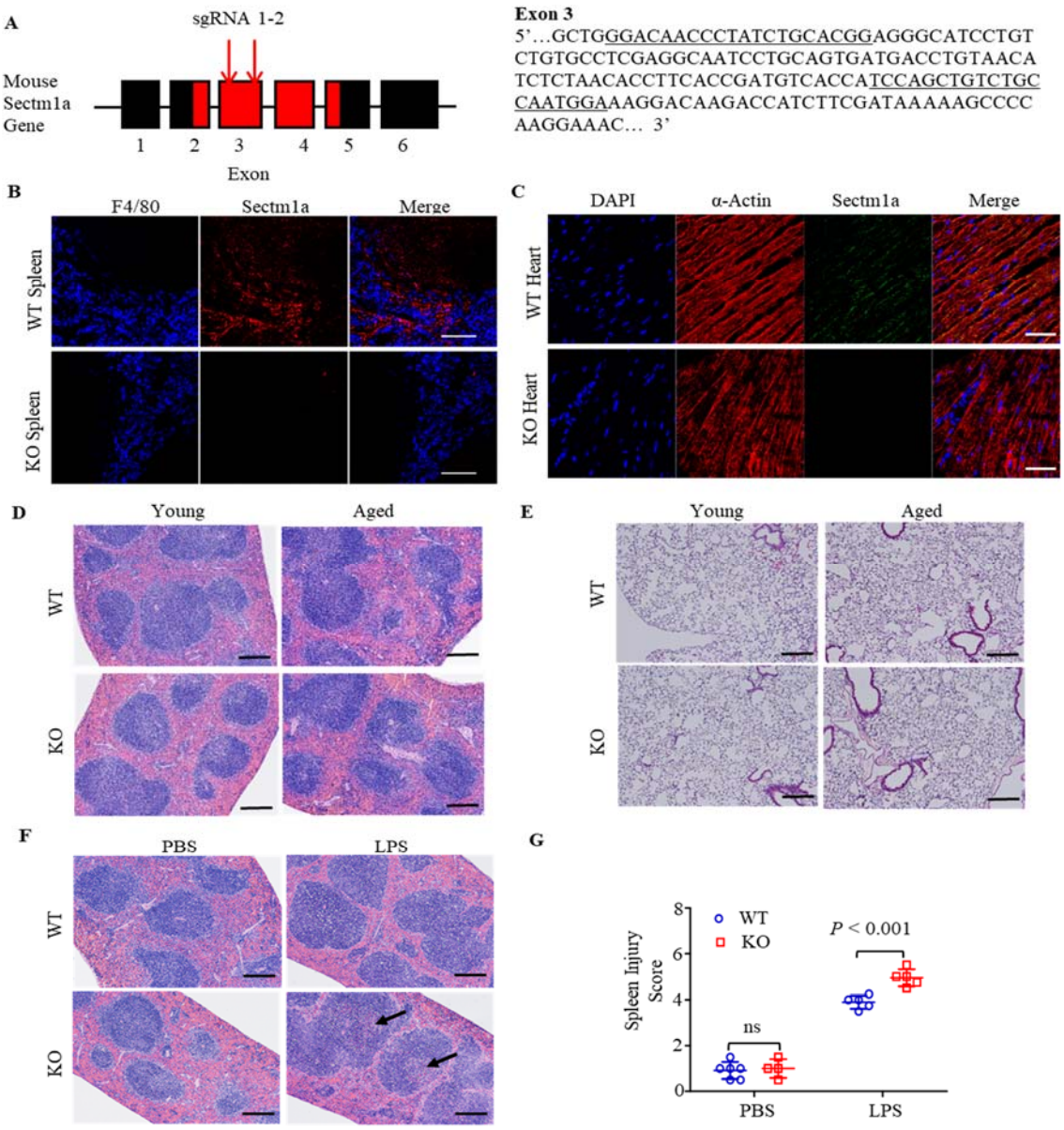

Figure S2. (A) Generation of Sectm1a-knockout mouse model. Two sgRNAs targeting to Exon3 of Sectm1a were selected to inject with Cas9mRNA into one-cell embryos and sequence between the sgRNA targeting sites were deleted. The cutting site of Cas9 is indicated by arrow and the targeting sequence is underlined. (B) Representative immunofluorescence stain images for Sectm1a in spleens of WT and KO mice. F4/80 (Blue) and Sectm1a (Red). Scale bar: 100 μm. (C) Representative immunofluorescence stain images for Sectm1a (Green) in hearts of WT and KO mice. α-Actin (Red), Sectm1a (Green), DAPI (Blue). Scale bar: 50 μm. (D) Representative H&E staining images of spleen sections collected from WT and KO mice at different ages. Young (2 months old), Aged (12 months old). Scale bar: 200 μm. (E) Representative H&E staining images of lung sections collected from WT and KO mice at different ages. Young (2 months old), Aged (12 months old). Scale bar: 200 μm. (F) Representative H&E staining images of spleen sections collected from WT and KO mice at 24 h after PBS or LPS injection. Scale bar: 200 μm. Arrows indicate germinal centers. (G) Injury scores for spleen.

Figure S3

A

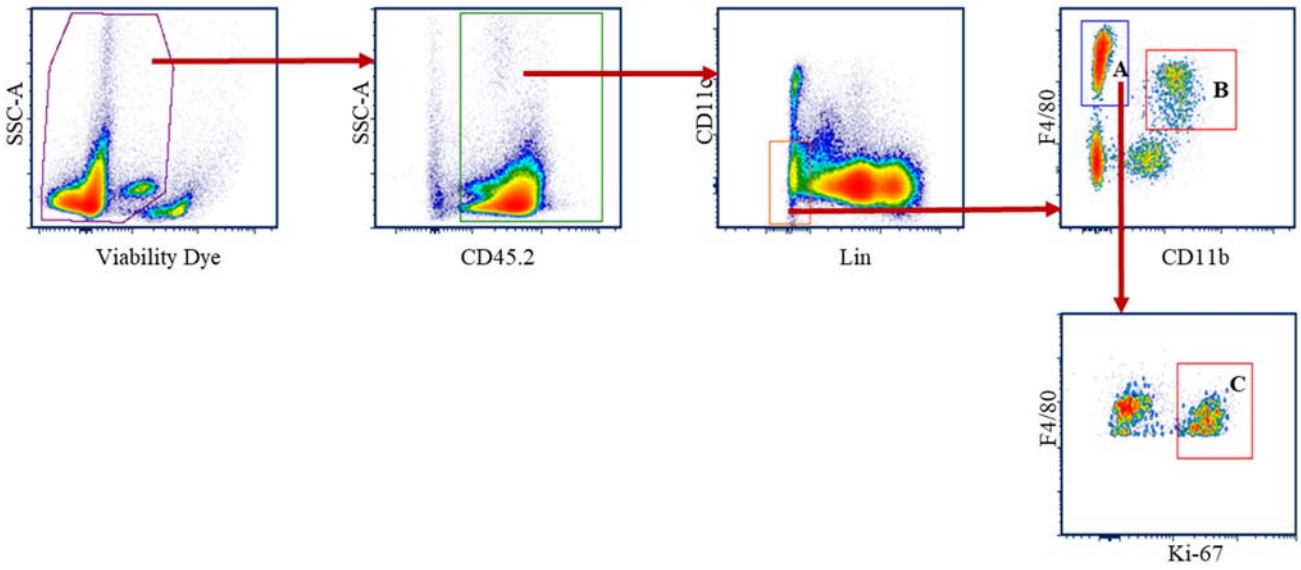

Figure S3A. Flow cytometry gating strategy used to identify leukocyte subsets in the mouse spleen following PBS or LPS injection. Single alive cell were subjected to a sequential gating strategy. Leukocytes were distinguished on the basis of CD45.2 expression and antibodies to specific markers (as outlined in Table S3) were used to identify red pulp macrophages (RPMs) (A: $CD45.2^{+}$ Lin^{-} $CD11c^{-}$ $F4/80^{++}$ $CD11b^{low/-}$) and splenic monocytes (B: $CD45.2^{+}$ Lin^{-} $CD11c^{-}$ $F4/80^{+}$ $CD11b^{++}$). RPMs undergoing proliferation were stained by Ki-67 (C: $CD45.2^{+}$ Lin^{-} $CD11c^{-}$ $F4/80^{++}$ $CD11b^{low/-}$ $Ki\text{-}67^{+}$).

Figure S3

B

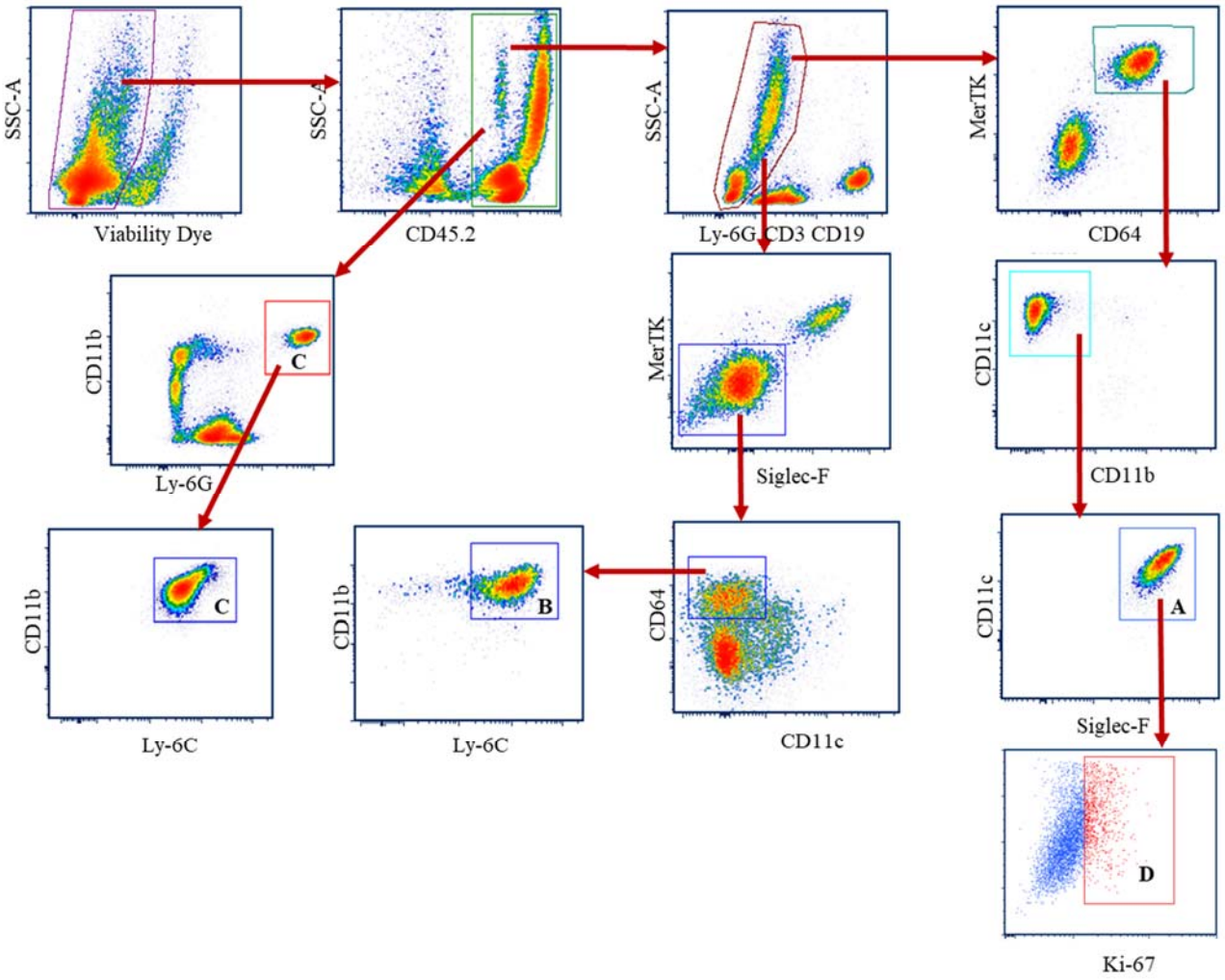

Figure S3B. (B) Flow cytometry gating strategy used to identify leukocyte subsets in the mouse lung following PBS or LPS injection. Single alive cell were subjected to a sequential gating strategy. Leukocytes were distinguished on the basis of CD45.2 expression and antibodies to specific markers (as outlined in Table S3) were used to identify alveolar macrophages (AMs) (A: $CD45.2^{+}$ $Ly\text{-}6G^{-}$ $CD3^{-}$ $CD19^{-}$ $MerTK^{+}$ $CD64^{+}$ $CD11c^{+}$ $Siglec\text{-}F^{+}$ $CD11b^{-}$), inflammatory monocytes (B: $CD45.2^{+}$ $Ly\text{-}6G^{-}$ $CD3^{-}$ $CD19^{-}$ $MerTK^{-}$ $Siglec\text{-}F^{-}$ $CD64^{+}$ $CD11b^{+}$ $Ly\text{-}6C^{+}$) and neutrophils (C: $CD45.2^{+}$ $Ly\text{-}6G^{+}$ $CD11b^{+}$ $Ly\text{-}6C^{+}$). AMs undergoing proliferation were stained by Ki-67 (D: $CD45.2^{+}$ $Ly\text{-}6G^{-}$ $CD3^{-}$ $CD19^{-}$ $MerTK^{+}$ $CD64^{+}$ $CD11c^{+}$ $Siglec\text{-}F^{+}$ $CD11b^{-}$ $Ki\text{-}67^{+}$).

Figure S3

C

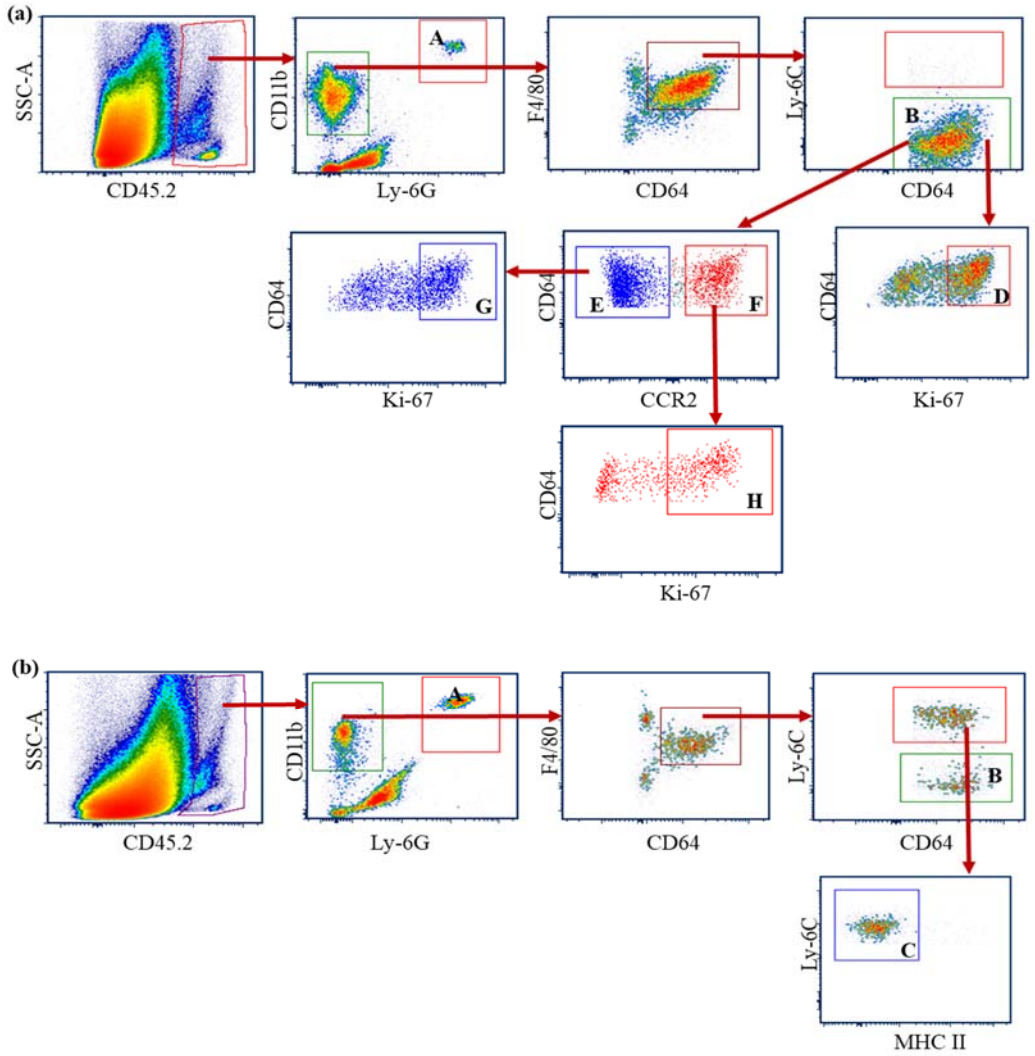

Figure S3C. (C) Flow cytometry gating strategy used to identify leukocyte subsets in the mouse heart following PBS [upper (a)] or LPS injection [lower (b)]. At 18 h post injection, cells were enzymatically and mechanically dissociated to produce single cell suspensions. Using a sequential gating strategy, leukocytes were distinguished on the basis of CD45.2 expression and antibodies to specific markers (as outlined in Table S3) were used to identify cardiac resident macrophage (B: $CD45.2^+$ $Ly\text{-}6G^-$ $F4/80^+$ $CD64^+$ $CD11b^+$ $Ly\text{-}6C^-$), inflammatory monocytes (C: $CD45.2^+$ $Ly\text{-}6G^-$ $F4/80^+$ $CD64^+$ $CD11b^+$ $Ly\text{-}6C^+$ $MHCII^-$) and neutrophils (A: $CD45.2^+$ $Ly6G^+CD11b^+$). The cardiac resident macrophages undergoing proliferation were stained by Ki-67 (D: $CD45.2^+$ $Ly\text{-}6G^-$ $F4/80^+$ $CD64^+$ $CD11b^+$ $Ly\text{-}6C^-$ $Ki\text{-}67^+$). The cardiac resident macrophages were subdivided into $CCR2^-$ macrophage (E: $CD45.2^+$ $Ly\text{-}6G^-$ $F4/80^+$ $CD64^+$ $CD11b^+$ $Ly\text{-}6C^-$ $CCR2^-$) and $CCR2^+$ macrophage (F: $CD45.2^+$ $Ly\text{-}6G^-$ $F4/80^+$ $CD64^+$ $CD11b^+$ $Ly\text{-}6C^-$ $CCR2^+$). These two subtype macrophages undergoing proliferation were identified as $Ki\text{-}67^+$ $CCR2^-$ CRM (Type G) and $Ki\text{-}67^+$ $CCR2^+$ CRM (Type H).

Figure S4

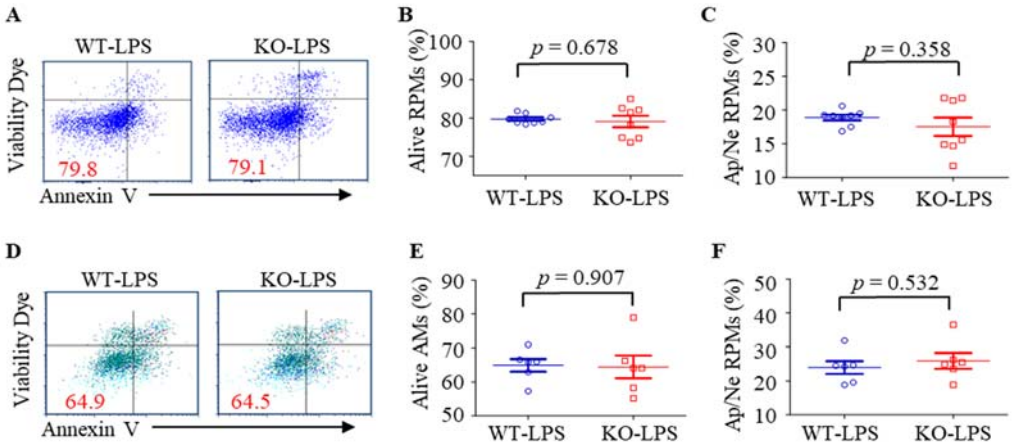

Figure S4. The spleen, lung and heart in WT and Sectm1a-KO mice were collected and subjected to flow cytometry analysis at 16 h after the administration of PBS or LPS (10 μg/g). For apoptosis/necrosis analysis, single cells isolated from the spleen and lung were stained with LIVE/DEAD fixable dye and Annexin V. (A-C) Representative flow cytometry plots (A) and quantification of live (B) as well as apoptosis/necrosis (Ap/Ne) population (C) within RPM after LPS injection. (n = 8). (D-F) Representative flow cytometry plots (D) and quantification of live (E) as well as apoptosis/necrosis population (F) within AM after LPS injection. (n = 6).

Figure S5

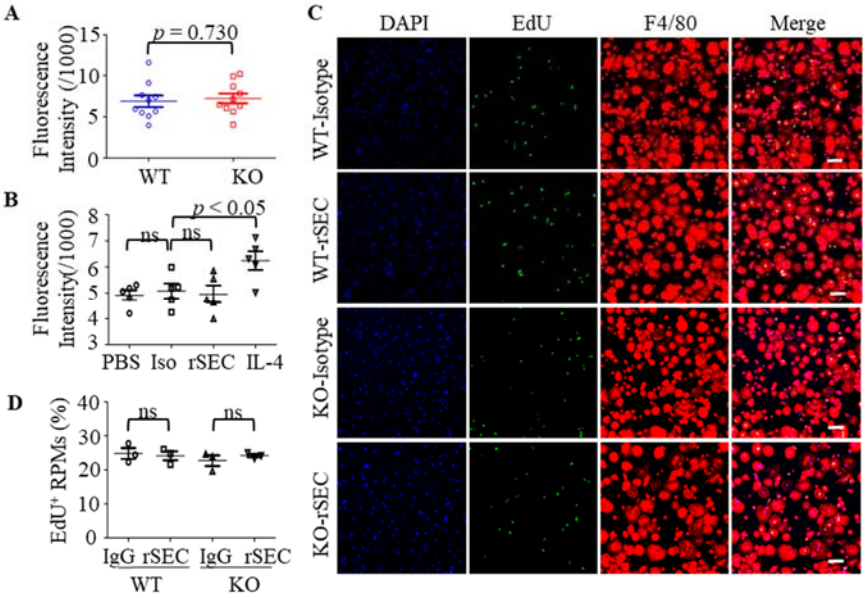

Figure S5. RPMs were isolated from WT and KO mouse spleens and stained with CellTracker™ Green CMFDA to reflect the cell number in each well. (A) After 48 h culture, fluorescence intensities of RPMs were compared between WT-RPMs and KO-RPMs (n = 10). (B) RPMs isolated from WT were stimulated with IgG2a (500 ng/ml) (Iso), rSectm1a (800 ng/ml) (rSEC) or IL-4 (200 ng/ml) for 48 h and fluorescence intensities of RPMs were compared. n = 5. (C and D) (C) EdU incorporation was assessed in RPM isolated from WT or KO mice after stimulation with IgG2a (1.25 μg/ml) or rSectm1a (2 μg/ml). Scale bar: 100 μm. (D) Percentages of EdU positive RPM in different treatment. Results are shown in means ± SEM of three independent experiments, and 400-600 cells were analyzed per experiment (n = 3).

Figure S6

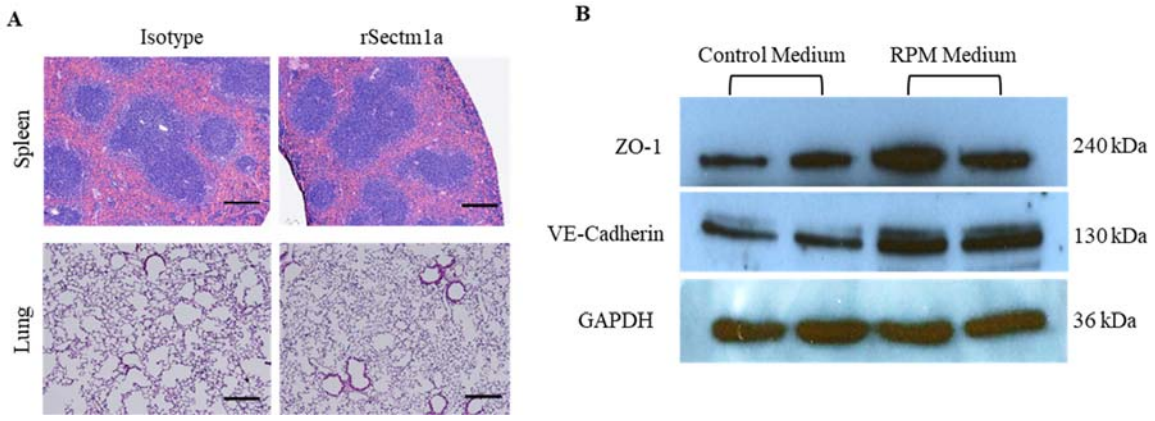

Figure S6. (A) WT mice were injected *i.v.* with IgG2a (125 μg/kg) (Isotype) or rSectm1a (200 μg/kg). The spleen and lung tissues were collected at 24 h post injection. Representative H&E staining images of spleen and lung sections. Scale bar: 200 μm. (B) MCECs were cultured in control medium or RPM conditioned medium for two days. Then, cells were collected for Western-blotting analysis of the expression levels of ZO-1 and VE-Cadherin. GAPDH was used as a loading control.

Supplemental tables

Table S1

Hematological data taken from young (2 months old) and aged (12 months old) WT mice.

	Young WT	Young KO	Aged WT	Aged KO
White blood cells ($\times 10^3/\mu l$)	2.8 ± 1.0	3.1 ± 0.7	2.5 ± 0.2	2.4 ± 0.4
Neutrophils ($\times 10^3/\mu l$)	0.5 ± 0.2	0.6 ± 0.1	0.5 ± 0.2	0.5 ± 0.1
Lymphocytes ($\times 10^3/\mu l$)	2.1 ± 0.7	2.3 ± 0.6	1.9 ± 0.2	1.8 ± 0.4
Monocytes ($\times 10^3/\mu l$)	0.2 ± 0.1	0.2 ± 0.1	0.1 ± 0.0	0.1 ± 0.1
Eosinophils ($\times 10^3/\mu l$)	0.0 ± 0.0	0.0 ± 0.0	0.0 ± 0.0	0.0 ± 0.0
Red blood cells ($\times 10^6/\mu l$)	8.5 ± 0.2	8.6 ± 0.3	8.2 ± 0.2	8.6 ± 0.3
Hemoglobin (g/dL)	13.6 ± 0.2	13.4 ± 0.4	12.5 ± 0.4	12.5 ± 0.5
Hematocrit (%)	46.1 ± 1.4	45.2 ± 1.6	41.3 ± 2.6	42.9 ± 1.3
MCV (fL)	53.2 ± 3	52.6 ± 0.7	50.7 ± 3.7	50.2 ± 1.7
Platelets ($\times 10^3/\mu l$)	1046.6 ± 117.5	983.8 ± 23.6	1240.6 ± 108.9	1165.8 ± 70.3

Blood were obtained from the heart and analyzed by Hemavet. Statistical analysis was carried out with Student's t-test. MCV (mean corpuscular volume).

Table S2

Hematological data taken from IgG2a-treated and Sectm1a-treated WT mice. IgG2a (125 µg/kg) (Isotype), Sectm1a (200 µg/kg)

	IgG2a	Sectm1a
White blood cells ($\times 10^3/\mu l$)	3.4 ± 0.8	3.7 ± 1.4
Neutrophils ($\times 10^3/\mu l$)	0.6 ± 0.2	0.7 ± 0.3
Lymphocytes ($\times 10^3/\mu l$)	2.5 ± 0.6	2.8 ± 1.1
Monocytes ($\times 10^3/\mu l$)	0.2 ± 0.1	0.21 ± 0.1
Eosinophils ($\times 10^3/\mu l$)	0.0 ± 0.0	0.01 ± 0.0
Red blood cells ($\times 10^6/\mu l$)	8.0 ± 0.4	8.32 ± 0.6
Hemoglobin (g/dL)	12.5 ± 0.5	13.2 ± 0.9
Hematocrit (%)	43.3 ± 2.2	43.2 ± 2.8
MCV (fL)	52.3 ± 1.3	53.3 ± 1.2
Platelets ($\times 10^3/\mu l$)	1083.0 ± 129.7	1126 ± 171.1

Blood were obtained from the heart and analyzed by Hemavet. Statistical analysis was carried out with Student's t-test. MCV (mean corpuscular volume).

Table S3. Key resource table

Table S4. Characteristics of human subjects

	Healthy Controls	Sepsis Patients
Variable	n = 34	n = 27
Age (years) ± SD	40 ± 16	58 ± 17
Male Gender (%)	17 (50%)	16 (59%)
White Race (%)	25 (74%)	15 (56%)
Source of Infection (%)	N/A	
Urinary Tract		8 (30%)
Pneumonia		9 (33%)
Intravascular Device		3 (11%)
Other		7 (26%)
Organism (%)	N/A	
Gram Neg Bacteria		7 (26%)
Gram Pos Bacteria		4 (15%)
Unknown		9 (33%)
Other		7 (26%)
Mechanical Ventilation (%)	N/A	10 (37%)
APACHE II Score ± SD	N/A	23.4 ± 8.0
Death (%)	N/A	12 (44%)

SD standard deviation, N/A not applicable, APACHE acute physiology and chronic health evaluation

Supplemental methods

Mice

C57BL/6 mice (WT) and GITR-KO (Tnfrsf18$^{-/-}$) mice were purchased from Jackson Laboratories (Bar Harbor, ME, USA). The global Sectm1a-KO mouse model on the C57BL/6 background was generated by the Division of Developmental Biology at Cincinnati Children's Hospital Medical Center through using the CRISPR/Cas9 system (Supplemental Figure S2A).[1] Male and female mice between 6 and 10 weeks of age were used for experiments in a gender-matched manner. For generating acute inflammation model, animals received indicated dose (5 μg/g, 10 μg/g or 20 μg/g of body weight) of LPS intraperitoneally (*i.p.*) in 0.2 ml phosphate buffered saline (PBS). For survival experiments, mice immediately received IgG2a (125 μg/kg) (Isotype) or rSectm1a (200 μg/kg) through intravenous injection (*i.v.*) after LPS injection. The survival rate of WT and KO mice were monitored every 6 h for a 96 h period after LPS injection. To pre-deplete tissue-resident macrophages, WT mice were injected (*i.v.*) with clodronate-liposome (200 μl, clodronate 5 mg/ml) or vehicle-liposome (200 μl, no clodronate) (control group).[2]

Isolation of naïve CD4 T cells and CD4 T cells

We disrupt spleen in PBS containing 2% fetal bovine serum (FBS). Remove aggregates and debris by passing cell suspension through a 70 μm mesh nylon strainer. Centrifuge at 500 x g for 5 minutes and re-suspend at 1 x 10^8 nucleated cells/ml in RPMI-1640 containing 10% fetal bovine serum (heat inactivated) and 1% Penicillin/Streptomycin Solution, 100 x (Corning). Following the protocol, naïve CD4 T cells and CD4 T cell were isolated from the cell suspension by negative selection, and unwanted cells are targeted for removal with biotinylated antibodies and streptavidin-coated magnetic particles. This negative selection is fast and untouch the

isolated cells, which benefit the following experiments. After isolation, the live naïve CD4 T cells were counted with 0.2% trypan blue dye and grown in the insert of transwell (1.5×10^6/well). The live CD4 T cells were also counted and plated in 12-well plates (3×10^6/well).

Preparation of red pulp macrophages (RPMs) from spleen

Mice were terminally anesthetized, and the spleen was carefully excised and thoroughly minced in PBS containing 3% FBS. The cell suspension was filtered through 70 μm Nylon cell strainer. Then, cells were pelleted by centrifuging 500 x g for 5 min at 4°C. To lysing red blood cells (RBCs), cell pellets were suspended in RBC lysis buffer (Biolegend) for 4 min at room temperature (RT) and pelleted again. The resulting cell pellet was re-suspended in DMEM (Corning) containing 10% FBS, 10 mM HEPES and 1% penicillin/streptomycin solution (100 x). Cells were counted and seeded on 100 mm dish (5×10^7/well) or on the coverslip coated with collagen in 12-well plates at the same density (5×10^6/well). These cells were allowed to attach and grow for 6 days. Then, cells were washed with warm PBS for three times to dump these unattached cells and culture medium was replaced by fresh one. After one day, cells were collected and used for the following experiments such as FACs or co-culture experiments.

Endothelial cell culture

Mouse Cardiac Endothelial Cells (MCECs) (5×10^5 cells/well) were cultured in 12-well plate with DMEM containing 10 mM penicillin/streptomycin, 10 mM HEPES and 5% FBS or RPM conditioned medium for 2 days. After two-day culture, MCECs were washed two times with warm PBS, then lysed for RNA isolation. To observe the change of ZO-1 linear pattern after stimulation, MCECs were seeded on the coverslip coated with collagen in 24-well plates at the same density (3×10^5 cells/well) and grown for two days with normal medium or RPM conditioned medium. Then, thrombin (3 U/ml) or PMA (40 ng/ml) were used to stimulate MCECs for 0.5 h. MCECs were washed with warm PBS and fixed by 4% Paraformaldehyde (PFA) solution in PBS.

To produce RPM conditioned media, the general medium (DMEM containing 10 mM penicillin/streptomycin, 10 mM HEPES and 5% FBS) was used as a starter general culture medium. 2×10^6 RPMs (for RPM medium) and 2×10^6 MCECs (for control medium) were respectively cultured in a 100 mm cell culture dish with 12 ml general medium at 37 °C in a 5 % CO_2 incubator. After 3 days of cultivation, the cell culture supernatant was collected. Debris was removed by centrifugation at 700 x g for 5 minutes. Then, FBS was added into supernatants (RPM conditioned medium or control medium) with 1:20 ratio (FBS: supernatant) in volume. These media were aliquoted and stored at −20 °C until use.

Flow cytometry analysis

Spleen cell suspensions were prepared from the excised spleens by mechanical disruption in PBS containing 2% FBS. Remove aggregates and debris by passing cell suspension through a 70 μm mesh nylon strainer. To prepare single cell suspension from the lung and heart, mice were terminally anesthetized and perfused with 20 mL PBS via cardiac injection. Lung and heart tissues were finely minced with scissors before digestion. The lung tissue was digested with RPMI-1640 solution containing 2 mg/ml collagenase type IV (Stemcell) and Deoxyribonuclease I (DNase I), 100 U/ml (Stemcell).[3] The heart tissue was subjected to enzymatic digestion with 450 U/ ml collagenase I (Sigma-Aldrich), 125 U/ml collagenase XI (Sigma-Aldrich), 60 U/ml hyaluronidase (Sigma-Aldrich) and 50 U/ml DNase I (Stemcell).[4] After 30-40 mins incubation at 37°C under 200 rpm agitation, lung tissues were passed through 70 μm cell strainer. Heart tissues were firstly passed through 100 μm cell strainer, and, then passed through 40 μm cell strainer. After removing aggregates and debris, all cell suspension were centrifuged at 500 x g for 5 minutes at 4°C and red blood cells were lysed with 3 ml of lysis buffer (Biolegend), incubated for 4 min at room temperature, and, then, diluted and washed with PBS.

For surface marker staining, we used the following mouse antibodies: FITC-conjugated CD45.2 (clone 104), lineage markers [eFlour 450-conjugated CD19 (clone 1D3), eFlour 450-conjugated NK1.1(clone PK136), eFlour 450-conjugated CD90.2 (clone 53-2.1), eFlour 450-conjugated CD49b (clone DX5), eFlour 450-conjugated CD3 (clone 17A2), Brilliant Violet 421-conjugated Ly-6G (clone 1A8)], APC-conjugated F4/80 (clone BM8), BV786-conjugated CD64 (clone X54-5/7.1), PE-conjugated CD11b (clone M1/70), PerCP-Cyanine5.5-conjugated CD11c (clone N418), PE/Dazzle 594-conjugated Ly-6C (clone HK1.4), APC-conjugated MERTK (clone DS5MMER), Alexa Fluor 700-conjugated Siglec F (clone 1RNM44N), PE-Cyanine5-conjugated MHC Class II (clone M5/114.15.2), Alexa Fluor 700-conjugated CCR2 (clone 475301), PerCP-Cyanine5.5-conjugated CD4 (clone RM4-

5), APC-eFluor 780-conjugated CD11b (clone M1/70), Alexa Fluor 647-conjugated F4/80 (clone BM8), PerCP-Cyanine5.5-conjugated CD45.2 (clone HK1.4), PE-Cyanine7-conjugated CD11c (clone N418).

For staining of intracellular Ki-67, cells from the lung and heart were fixed and permeabilized with Foxp3 / Transcription Factor Staining Buffer Set (Invitrogen), washed with Intracellular Staining Perm Wash Buffer, and stained with BV605-conjugated anti-mouse Ki-67 (clone XMG1.2, BioLegend). For staining of intracellular Ki-67 in RPM, cells from the spleen were fixed by 2% PFA and permeabilized with 0.1% Triton in PBS, washed the cells with 2 mL of PBS (containing 0.1% triton), and stained with BV605-conjugated anti-mouse Ki-67 (clone XMG1.2, BioLegend). For measurement of intracellular cytokine expression of T cells , cells were isolated stimulated with 20 ng/ml phorbol-12-myristate 13-acetate (PMA, Stemcell) and 1 μg/mL ionomycin (Stemcell) in the presence of BD GolgiStop (BD Pharmingen) for 5 h. Cells were subsequently stained with mouse Th1/Th2/Th17 phenotyping kit (BD Pharmingen) according to the manual. The apoptosis and necrosis of RPMs and AMs were evaluated with Annexin V Apoptosis Detection Kit (eBioscience) following the manual. In all experiments, doublet cells were excluded by SSC-A and FSC-A gating followed by FSC-H and FSC-A gating. Samples were run on BD LSRII) and the data were analyzed with FCS express V6 (De Novo Software, USA).

Immunofluorescence stain

The mouse spleen was embedded in O.C.T. compound (Fisher HealthCare) and frozen in liquid nitrogen. Spleens were then sectioned at a thickness of 7 μm with a cryostat, and fixed with 4% PFA at room temperature. The sections were then permeabilized with 0.2% tween 20 (ThermoFisher Scientific) and blocked with 1% bovine serum albumin (BSA) for 1 h and incubated with the primary antibodies (Pacific Blue-conjugated anti-mouse F4/80 and Alexa Fluor 647-conjugated anti-mouse Ki-67) diluted in 1% BSA in PBS overnight at 4°C. Sections were washed three times with PBS and mounted with ProLong Diamond Antifade Mounting medium (Invitrogen). For the immunofluorescence staining of RPMs and MCECs treated with (Thrombin or PMA), cells were fixed on the coverslip, blocked with 1% BSA and incubated with primary antibody (PE-conjugated anti-mouse F4/80 or ZO-1 antibody) diluted in 1% BSA in PBS overnight at 4°C. After washing, MCECs were incubated with secondary antibody, Alexa flour 488-conjugated anti-Rabbit IgG, at room temperature for 1 h. Thereafter, cells were washed three times with PBS and mounted with ProLong diamond Antifade Mounting medium with DAPI (Invitrogen). Images were captured with Zeiss LSM710 LIVE Duo Confocal Microscope (Live Microscopy Core, University of Cincinnati)

Measurement of vascular leakage in multiple organs

The pulmonary microvascular permeability was determined in each experimental group by measuring the Evans blue (EB) accumulation in lung tissue and lung wet to dry weight ratio. The Evans blue dye assay was performed as described previously.[5] Briefly, the mice were administered 1% EB solution (Sigma, St. Louis, MO, USA) in PBS via tail vein injection. After 30 min, mice were sacrificed and perfused via the heart, and the lung tissues were collected. The lung weights were measured and placed in 1 ml of formamide (Avantor, Center Valley, PA, USA) at 60 °C for 24 h to extract EB. Absorbance was measured at 620 nm, and EB concentration was determined from a standard curve. To measure the wet to dry weight ratio of lung, the left lung was harvested and weighed to measure a wet weight in each group. The wet lung was then dried in an oven at 60 °C for 48 h and re-weighed as dry weight. The ratio of wet weight to dry weight of the lung was calculated. The wet to dry weight ratio of spleen was measured and calculated in the same way.

For the measurement of cardiac vascular permeability, EB accumulation in heart was determined as described previously.[6] Briefly, mice were sacrificed and perfused with 30 ml of PBS through the left ventricle after administration of EB, and conducted following experiment as described previously (. Heart was removed and frozen in O.C.T compound. Frozen sections (7-μm in thickness) were fixed and observed under a confocal microscope, Zeiss LSM710 LIVE Duo Confocal Microscope (Live Microscopy Core, University of Cincinnati). The intensity of Evans blue fluorescence (excitation at 620 nm, emission at 680 nm) corresponding to the amount of dye in extravascular compartment was quantified with Image J software (Wayne Rasband, National Institutes of Health, Bethesda, MD).

Spleen/lung histology and injury score

The spleen and lung tissues were collected from mice at 24 h post-LPS injection. All the lung were perfused via the heart, inflated and fixed with 10% buffered formalin for more than two days, followed by embedded in paraffin, and cut into 5-μm sections. Tissue sections were stained with hematoxylin and eosin (H&E), examined with a light microscope (Olympus, Japan), and scored by a pathologist who was blinded to the experimental groups. To evaluate

the lung jury, 6-8 independent random lung fields were evaluated per mouse for neutrophils in alveolar spaces, neutrophils in the interstitial spaces, hyaline membranes, proteinaceous debris filling the airspaces, and alveolar septal thickening and weighted according to the relevance ascribed by the official American Thoracic Society workshop report on features and measurements of experimental acute lung injury in animals.[7] Segments of spleen were separately scored for the enlargement of white pulp areas and for the presence of germinal centers according to the description in the previous report.[8]

Acquisition of human blood samples

This study was approved by the Institutional Review Board at the Medical University of South Carolina. We screened all new intensive care unit (ICU) admissions at a single tertiary-care academic hospital from July 2013 to February 2015 for the presence of severe sepsis based on the American College of Chest Physicians/Society of Critical Care Medicine consensus definition.[9] Additional inclusion criteria included age ≥18 years and admission into the ICU within the previous 24 hours. We excluded immunocompromised patients as defined by: immunosuppressive medication use, leukopenia, current hematologic malignancy, and history of stem cell transplant, and excluded patients transferred in from other hospitals if they had spent > 24 hours in an ICU at the time of screening. Patients who had transitioned to comfort measures only at the time of screening were further excluded. Healthy control subjects were recruited through local advertising. Informed consent for study participation and publication of results was obtained from all research subjects or their legally authorized representatives. Demographic and clinical information from septic patients was abstracted from the electronic medical record including the source and type of infection as well as variables required to calculate acute physiology and chronic health evaluation (APACHE) II scores (Table S4). Discharge destination and vital status were similarly captured. Basic demographics were recorded from healthy controls (Table S4). Consenting subjects had blood drawn via venipuncture or from pre-existing intravascular catheters. Blood samples from septic patients were collected within 24 hours of admission to the ICU. Samples were centrifuged at 3400 × g for 10 minutes and the plasma supernatant was collected and stored in aliquots at -80 degrees Celsius.

Supplemental references

1. Li, Y., Deng, S., Wang, X., Huang, W., Chen, J., Robbins, N., et al. (2020). Sectm1a Deficiency Aggravates Inflammation-Triggered Cardiac Dysfunction through Disruption of LXRα Signaling in Macrophages. Cardiovasc. Res. doi: 10.1093/cvr/cvaa067.
2. Palermo, M.S., Alves, R., Rooijen, V., and Isturiz, M.A. (1999). Depletion of liver and splenic macrophages reduces the lethality of Shiga toxin-2 in a mouse model. Clin. Exp. Immunol. *116,* 462-467.
3. Jungblut, M., Oeltze, K., Zehnter, I., Hasselmann, D., and Bosio, A. (2009). Standardized preparation of single-cell suspensions from mouse lung tissue using the gentleMACS Dissociator. J. Vis. Exp. *29*, 1266.
4. Hulsmans, M., Sager, H.B., Roh, J.D., Valero-Muñoz, M., Houstis, N.E., Iwamoto, Y., et al. (2018). Cardiac macrophages promote diastolic dysfunction. J. Exp. Med. *215*, 423-440.
5. Reutershan, J., Morris, M.A., Burcin, T.L., Smith, D.F., Chang, D., Saprito, M.S., et al. (2006). Critical role of endothelial CXCR2 in LPS-induced neutrophil migration into the lung. J. Clin. Invest. *116*, 695-702.
6. Castanares-Zapatero, D., Bouleti, C., Sommereyns, C., Gerber, B., Lecut, C., Mathivet, T., et al. (2013). Connection between cardiac vascular permeability, myocardial edema, and inflammation during sepsis: role of the α1AMP-activated protein kinase isoform. Crit. Care Med. *41*, 411-422.
7. Matute-Bello, G., Downey, G., Moore, B.B., Groshong, S.D., Matthay, M.A., Slutsky, A.S., et al. (2011). An official American Thoracic Society workshop report: features and measurements of experimental acute lung injury in animals. Am. J. Respir. Cell Mol. Biol. *44*, 725-738.
8. Giamarellos-Bourboulis, E. J., Tziortzioti, V., Koutoukas, P., Baziaka, F., Raftogiannis, M., Antonopoulou, A., et al. (2006). Clarithromycin is an effective immunomodulator in experimental pyelonephritis caused by pan-resistant Klebsiella pneumoniae. J Antimicrob Chemother. *57*, 937–944.
9. Bone, R.C., Balk, R.A., Cerra, F.B., Dellinger, R.P., Fein, A.M., Knaus, W.A., et al. (1992). Definitions for sepsis and organ failure and guidelines for the use of innovative therapies in sepsis. Chest *101*, 1644-1655.